Free Radical Biology and Medicine 198 (2023) 92–108

Contents lists available at ScienceDirect

Free Radical Biology and Medicine

journal homepage: www.elsevier.com/locate/freeradbiomed

NOX2 and NOX4 control mitochondrial function in chronic myeloid leukaemia

Marta Romo-González [a,b], Carla Ijurko [a,b], María Teresa Alonso [c], Marta Gómez de Cedrón [d], Ana Ramirez de Molina [d], María Eugenia Soriano [e], Ángel Hernández-Hernández [a,b,*]

[a] Departamento de Bioquímica y Biología Molecular, Universidad de Salamanca, Salamanca, 37007, Spain
[b] IBSAL (Instituto de Investigación Biomédica de Salamanca), Salamanca, 37007, Spain
[c] Instituto de Biología y Genética Molecular (IBGM), Universidad de Valladolid and Consejo Superior de Investigaciones Científicas (CSIC), Valladolid, 47003, Spain
[d] Molecular Oncology Group, IMDEA Food Institute, CEI UAM + CSIC, Madrid, Spain
[e] Department of Biology, University of Padova, Padova, 35121, Italy

ARTICLE INFO

Keywords:
NOX2
NOX4
Chronic myeloid leukaemia
Mitochondria
Metabolism
Oxidative phosphorylation

ABSTRACT

Cancer cells are characterised by an elevated metabolic plasticity and enhanced production of reactive oxygen species (ROS), two features acknowledged as hallmarks in cancer, with a high translational potential to the therapeutic setting. These aspects, that have been traditionally studied separately, are in fact intimately intermingled. As part of their transforming activity, some oncogenes stimulate rewiring of metabolic processes, whilst simultaneously promoting increased production of intracellular ROS. In this scenario the latest discoveries suggest the relevance of nicotinamide adenine dinucleotide phosphate (NADPH) oxidases (NOX) to connect ROS production and metabolic control. Here we have analysed the relevance of NOX2 and NOX4 in the regulation of metabolism in chronic myeloid leukaemia (CML), a neoplasia driven by the expression of the breakpoint cluster region-Abelson fusion oncogene (*BCR-ABL*). Silencing of NOX2 enhances glycolysis and oxidative phosphorylation rates, together with an enhanced production of mitochondrial ROS and a decrease in mitochondrial DNA copy number, which reflects mitochondrial dysfunction. NOX4 expression was upregulated upon NOX2 silencing, and this was required to alter mitochondrial function. Our results support the relevance of NOX2 to regulate metabolism-related signalling pathways downstream of BCR-ABL. Overall we show that NOX2, through the regulation of *NOX4* expression, controls metabolism and mitochondrial function in CML cells. This notion was confirmed by transcriptomic analyses, that strongly relate both NOX isoforms with metabolism regulation in CML.

1. Introduction

Almost a century ago Otto Warburg realized that most cancer cells relied on glycolysis rather than in oxidative phosphorylation (OXPHOS) as a main source of energy [1]. It is surmised that this aerobic glycolysis would provide a fast ATP synthesis and a source of intermediates for anabolic purposes. Although many tumour cells respond to this pattern, cancer cells show a high metabolic plasticity, providing a great variety of metabolic adaptations [2].

On the other hand, tumour cells show an enhanced level of reactive oxygen species (ROS) [3], which might contribute to cellular transformation due to their ability to induce DNA damage [4]. ROS can also activate signalling pathways that promote cell growth [5] and the escape from apoptosis [6].

Metabolic rewiring and the enhanced levels of ROS are acknowledged as hallmarks in cancer. They have been intensively studied due to their therapeutic potential [7,8], however, in most cases as independent entities. Nevertheless, it is well known that intracellular ROS levels are strongly determined by the activity of metabolic pathways, as well as that ROS modulate both directly and indirectly master regulators and key enzymes of metabolism [2].

Oncogenes, which have been the intense focus of cancer researchers for decades, show a tight association with metabolic alterations and ROS production [9]. This is the case of chronic myeloid leukaemia (CML) which is caused by the expression of breakpoint cluster region-Abelson fusion oncogene (*BCR-ABL*), a constitutive active kinase that comes from

* Corresponding author. Plaza Doctores de la Reina, s/n, P.O.37007, Salamanca, Spain.
E-mail address: angelhh@usal.es (Á. Hernández-Hernández).

https://doi.org/10.1016/j.freeradbiomed.2023.02.005
Received 19 December 2022; Received in revised form 31 January 2023; Accepted 7 February 2023
Available online 9 February 2023

the Philadelphia chromosome as result of the genetic translocation (t (9; 22)) [10]. BCR-ABL has a strong regulatory effect on metabolism. In CML bulk cells this kinase induces a high glucose dependence thereby producing a great amount of pyruvate; some of it will enter into the tricarboxylic acid (TCA) cycle at the same rate as in non-malignant cells, but the rest, a significant amount, will be transformed into lactate that will be secreted [11]. In contrast to healthy hematopoietic stem cells (HSC) and leukemic bulk cells, CML leukemic stem cells (LSC) besides increasing glycolysis, also appear to up-regulate OXPHOS [12]. On the other hand, BCR-ABL is associated with high levels of ROS either by an exacerbated cellular metabolism [13], as well as by an hyperactivation of ROS production-sources such mitochondria [14], xanthine oxidoreductase (XOR) [15], and nicotinamide adenine dinucleotide phosphate (NADPH) oxidases [16,17].

NADPH oxidases are the only cellular system specialized in the production of ROS [18]. Since their discovery, NADPH oxidases have been implicated in several important biological processes such immune defence, or cell differentiation. Recent reports support the relevance of some members of the family, especially NADPH oxidase 2 (NOX2) and NADPH oxidase 4 (NOX4) in the regulation of metabolism. NOX2 is involved in the regulation of the uptake of glucose [19], and it seems required to maintain a high glycolytic rate [20–22]. NOX4 behaves as a mitochondrial sensor [23], modulating mitochondrial dynamics [24].

We have previously shown the relevance of NADPH oxidases for maintaining BCR-ABL signalling pathway [17]. Given recent evidence sustaining a role of NADPH oxidases in the regulation of the cellular metabolism, together with the ability of BCR-ABL to induce metabolic rewiring and the production of ROS through NADPH oxidases, we reasoned that NADPH oxidases might play a key role in the control of CML metabolism. Therefore, here we have tested the role of NOX2 and NOX4 in the regulation of CML metabolism. Our results show that NOX2 silencing enhances glycolysis and OXPHOS rates, however, this is not translated into a more efficient metabolic process. Downregulation of NOX2 is accompanied by the upregulation of NOX4. We tested whether this was relevant for the mitochondrial alterations observed upon NOX2 silencing. Importantly, the mitochondrial parameters altered by NOX2 silencing were reversed after sequential knockdown of NOX4. In summary, our results strongly indicate that NOX2 and NOX4 are key in the metabolic homeostasis of CML cells, and establish a functional relationship between NOX2 and the mitochondria, regulated by NOX4.

2. Materials and methods

2.1. Cell culture

K562 cells were purchased from ECACC-European Collection of Authenticated Cell Cultures (Sigma Aldrich, Madrid, Spain), and grown in 10% FBS-supplemented RPMI medium (Biowest) plus 100 U/mL penicillin, 100 U/mL streptomycin, and 2 mmol/L L-glutamine (Biowest) at 37 °C and 5% CO_2. Cells were tested for Mycoplasma spp. Contamination prior to use with PlasmoTest detection kit (Invivo-Gen, cat #rep-pt1).

2.2. RNA interference

Silencing was performed by lentiviral transduction as previously [25,26]. Target sequences are detailed in Supplementary Table I. Silencing was checked by RT-qPCR or immunoblotting (Supplementary Fig. 1) [25,26].

2.3. qRT-PCR

qRT-PCR was performed as described in Ref. [17]. Briefly, total mRNA was purified using TRI Reagent (Sigma-Aldrich), its concentration and quality was determined in a NanoDrop 1000 spectrophotometer (Thermo Scientific) and 4 μg of total RNA was used for cDNA synthesis using SuperScript® II (Invitrogen). qPCR assays were performed using GoTaq qPCR Master Mix (Promega) in the StepOne Real-Time PCR System device (Applied Biosystems). Data were normalized to the housekeeping *ACTIN* mRNA levels. The specific DNA primers used are listed in Supplementary Table I.

2.4. mtDNA/nDNA

Genomic DNA was isolated by digesting 2×10^6 cells in 100 μL of lysis buffer (10 mM Tris-HCl pH 8; 0.4 M NaCl; 25 mM EDTA; 0.5% SDS (w/v), 0.2 mg/mL proteinase K) and incubated this mixture at 55 °C and shaking until the solution was no longer viscous. After incubation, the sample was completely purified by several extractions in phenol/chloroform pH 8. Genomic DNA was diluted in 8 mM NaOH with RNase-A 10 mg/mL, and its concentration and quality were determined in a NanoDrop 1000 spectrophotometer (Thermo Scientific). Quantification of the mitochondrial to nuclear DNA (mtDNA/nDNA) ratio was performed by qRT-PCR with the target sequences and conditions described before [27]. Oligonucleotides sequences are available in Supplementary Table I.

2.5. Immunoblotting

Total proteins cell extracts and mitochondria-enriched fraction were obtained as before [15,28]. Immunoblotting was done as previously [25,26]. The complete list of antibodies used is given in Supplementary Table II. Image acquisition was performed with ChemiDoc MP Imaging System (Bio-Rad) and bands quantification with Image Lab™ 6.0.1 (Bio-Rad) [15]. NOX4 monoclonal antibody (clone 20.3) was kindly provided by Dr. Ulla Knaus (University College Dublin) [29].

2.6. Metabolism analysis

RNAi cells were incubated for 2 h at 37 °C with 2 g/L D-glucose-$^{13}C_6$ (ChemCruz, sc-239643A). Metabolite extraction was carried out as previously described [30]. Extracellular glucose in the culture medium of unlabelled cells was also determined after 48 h. Separation and analysis were carried out by the General Mass Spectrometry Facility of the University of Salamanca. HPLC was performed using an XBridge amide column (Waters) (100 mm length x 2.1 mm inner diameter x 3.5 μm particle size) on a Waters Alliance HT HPLC system (Waters). The mobile phase A consisted of acetonitrile and mobile phase B was water/acetonitrile mixture 15/85 with 0.1% ammonia. The following gradient was applied: 95% A 5% B (0–10 min), 70% A 30% B (10–17.1 min), 95% A 5% B (17.1–20 min). Mass spectrometry was performed on a ZQ4000 quadrupole mass spectrometer, working in negative mode, with an ionisation voltage of 3.0 kV and a cone voltage of 20V. Acquisition was performed in scan range 50–500 amu. Metabolite analysis was performed in a random manner to reduce bias and systematic errors. Metabolite levels were normalized to protein concentration.

2.7. LDH activity

LDH activity was determined in duplicate on 5×10^5 cells with a commercial kit following the manufacturer's instructions (Sigma-Aldrich, MAK066) and normalized to protein concentration.

2.8. Determination of $NADP^+$ and NADPH concentrations

$NADP^+$ and NADPH concentrations were determinate in duplicate on 3 x 10^5 cells with the commercial kit MAK038 (Sigma-Aldrich), following the manufacturer's instructions and normalized to protein concentration.

2.9. Extracellular acidification rate (ECAR) and oxygen consumption rate (OCR) determination assays

Glycolytic function (*Glycolysis Stress Test)* and mitochondrial respiration (*MitoStress Test*) were carried out on 25,000 and 50,000 cells/well, respectively, in wells pretreated with Cell-Tak (Corning), following the manufacturer's instructions. For *Glycolysis Stress Test* were sequentially injected 10 mM glucose, 1.5 μM oligomycin and 50 mM 2-DG (2-Deoxy-D-glucose), measuring the ECAR at each point. For *MitoStress Test* 1.5 μM oligomycin, 0.9 μM FCCP (carbonyl cyanide 4-(trifluoromethoxy) phenylhydrazone), and 0.5 μM antimycin A/rotenone were sequentially injected, measuring the OCR at each point. All compounds used were purchased from Agilent Technologies. For data analysis we used Agilent Technologies Seahorse Wave software (Agilent). All experiments were performed in quintuplicate.

2.10. Mitochondrial respiration of isolated mitochondria

Mitochondria isolation and oxygen consumption were performed as previously described by Frezza et al. [28]. Briefly, oxygen consumption was measured using a Clark-type oxygen electrode (Hansatech Oxygraph) in 300 μl of KCl-experimental buffer containing the complex I substrates 5 mM Glutamate/2.5 mM Malate. Two minutes after mitochondria (150 μg) incubation, state 3 was induced by adding 200 μM ADP, and after 3 min, 1 μM oligomycin was also added. Uncoupled respiration was finally induced by adding 20 nM FCCP.

2.11. Measurements of mitochondrial membrane potential

7×10^5 cells were plated in 6 well plate coverslips pre-treated with 5 μg/ml of poli-D-lysine (Sigma-Aldrich). After 2 h, cells were incubated in HBSS containing 20 nM TMRM (tetramethylrhodamine methyl ester) (Molecular Probes) in presence of 1 μM cyclosporine H, at 37 °C, 30 min. Sequential images of TMRM fluorescence were acquired every minute using the iMIC-Andromeda system for 25 min. Data were normalized with complete depolarization obtained 10 min after 4 μM FCCP addition. TMRM fluorescence intensity was measured in at least 10 single cells randomly selected per experimental condition and five biological replicates. Analyses of the TMRM fluorescence of the mitochondrial regions of interest were carried out using the ImageJ software.

2.12. Mitochondria and MERCs morphometric analysis

Morphometric analysis was performed by Transmission Electron Microscopy (TEM) at the Electron Microscopy Facility of the University of Padova (Italy) using a Tecnai- G2 electron microscope (Philips-FEI) equipped with an Olympus Veleta side camera and a TVIPS F114 bottom camera. Samples were fixed and processed as described before [31]. Mitochondrial area, mitochondria number per cell, and number of mitochondria-ER contacts (MERCs) of at least 30 cells were quantified by using ImageJ software as previously [31]. We considered MERC when the distance between the two organelles was less than 50 nm.

2D Reconstructed Z-stacks from confocal images of TMRM labelled cells were processed using Fiji to reduce background and outline the mitochondrial network. The processing was performed in parallel in individual cells from the different lines. Mitochondrial length was measured by hand using the Freehand line tool and using arbitrary units (a.u.). 3D reconstructions were revised to confirm the phenotype.

2.13. Mitochondrial ROS and MitoTracker measures

Mitochondrial ROS levels and mitochondrial content were measured by labelling 500,000 cell with 5 μM MitoSOX™ Red (Invitrogen) or 250,000 cells with 200 nM MitoTracker™ Deep Red FM (Invitrogen) respectively, following the manufacturer's instructions. Cells were acquired with a Becton-Dickinson FACSCalibur cytometer (BD Biosciences) using CellQuest software (BD Biosciences). Median fluorescents intensity were analysed as before [32] using FlowJo V.10.5.3 (BD Biosciences).

2.14. Measurement of mitochondrial calcium

We measured mitochondrial calcium levels by luminescence of the Ca^{2+} sensor td-Tomato-aequorin (TA) with mitochondrial targeting (mitTA), kindly provided by Dr. María Teresa Alonso (IBGM, University of Valladolid, Spain). Stable K562 clones expressing mitTA were obtained by nucleofection (Neon™, Invitrogen) following manufacturer's instructions, and them silenced for NOX2, NOX4 or NOX2/NOX4, verifying TA localization at mitochondria by confocal microscopy. For measurements, 300,000 cells were seeded on poly-L-lysine (Sigma-Aldrich) coated 4-well plates for 16 h. Aequorin luminescence were done as previously described [33]. The calibration was performed for this probe as previously [33].

2.15. Cell proliferation

Proliferation was determined by MTT assay, as we have done previously [17]. Cells were seeded at a concentration of $2{,}5 \times 10^5$ cells/mL in glucose-free RPMI 1640 medium (Sigma-Aldrich, R1383) with 10% FBS supplemented with 2 g/L glucose (Sigma-Aldrich) or 10 mM galactose (Sigma-Aldrich). Proliferation was considered as the change in absorbance between day 0 and day 2 of cell culture. All experiments were performed by triplicate.

2.16. RNA seq analysis

cDNA libraries were compiled using the Illumina Truseq stranded mRNA LT Sample Prep Kit. Paired-end 150 nt length sequencing was performed on an NovaSeq 6000 from Illumina. RNAseq data can be found publicly available in the SRA database from NCBI with the submission localizer **PRJNA928236**.

Reads obtained were mapped on the Human reference genome GRCh38 using the bioinformatic facility tool of the University of Salamanca (https://ranaseq.eu/home). This bioinformatics tool carried out alignment and comparative genetic analysis of the samples, as well as an analysis of significantly altered processes and the gene set enrichment analysis (GSEA) through the GO database (Gene Ontology knowledgebase, https://geneontology.org/), and enriched pathways using the following databases: KEGG (https://www.genome.jp/kegg/pathway.html), REACTOME (https://reactome.org/) and WikiPathways (https://www.wikipathways.org/index.php/WikiPathways). Differential expression analysis was performed with DESeq2 using the Wald test and considering the data as paired to reduce data dispersion derived from independent experiments. Genes with an adjusted p-value <0.05 were considered as differentially expressed genes (DEGs).

2.17. Statistical analysis

Bar graphs show the mean of the data ± the standard error of the mean (SE) of "n" biological replicates. In dot graphs, each dot represents the result of a biological replicate, unless otherwise indicated in the figure caption, and the horizontal black line denotes the mean value of the experimental group. For comparisons between two groups, unpaired two-way Student's t-test was used. For comparisons of multiple groups, ANOVA test was performed; when the data adjusted to the normal distribution, we applied the appropriate post hoc in each case; or Kruskal-Wallis, when data did not adjust to the normal distribution. Data were analysed with SPSS 25 software. Statistical analyses for the RNA-Seq experiments are described in the relevant section. The symbols above the bars indicate the differences versus the corresponding control as shown in the figure caption; * vs control, + vs NOX2 RNAi and # vs NOX4 RNAi. Differences were considered statistically significant when

the p-value was less than 0.05 (*/+/#), 0.01 (**/++/##) or 0.001 (***/+++/###).

3. Results

3.1. Silencing of NOX2 enhances the use of glucose through the glycolytic pathway

BCR-ABL promotes the Warburg effect an enhances the production of ROS in leukemic cells [11,34]. We have previously shown that NADPH oxidases are required to maintain active the BCR-ABL signalling pathway [17]. Therefore, it can be surmised that redox signalling mediated by NADPH oxidases could be important for the metabolic control exerted by BCR-ABL. To test this hypothesis, we initially focused on NOX2, the most abundant isoform in hematopoietic cells. In the CML model cell line K562 we silenced the expression of two components of the NOX2 complex: the catalytic subunit NOX2, and its stabilising partner p22^{phox} (Supplementary Fig. 1). It worth mentioning that p22^{phox} also belongs to NOX1, NOX3 and NOX4 complexes, and therefore, its downregulation would presumably affect also to these NOX homologues.

To test the use of glucose, cells were incubated with medium containing 2 g/L D-glucose-$^{13}C_6$ for 2 h. NOX2-silenced cells showed a significant decrease in the concentration of extracellular ^{13}C-labelled glucose, suggesting an enhanced use of glucose by these cells. The same result was observed in the concentration of unlabelled glucose, and therefore in the total glucose concentration (Fig. 1A). In fact, after 2 days of culture the amount of extracellular glucose in the NOX2-silenced cells was reduced by more than a 70% with respect to control cells (Supplementary Fig. 2A).

NOX2-silenced cells also showed a significant decrease in the levels of the following intracellular ^{13}C-labelled metabolites: glucose (Fig. 1B), glucose-6-phosphate (Fig. 1C), and phosphoglycerate (Fig. 1D), and also in the total amounts of these metabolites. These results consistently

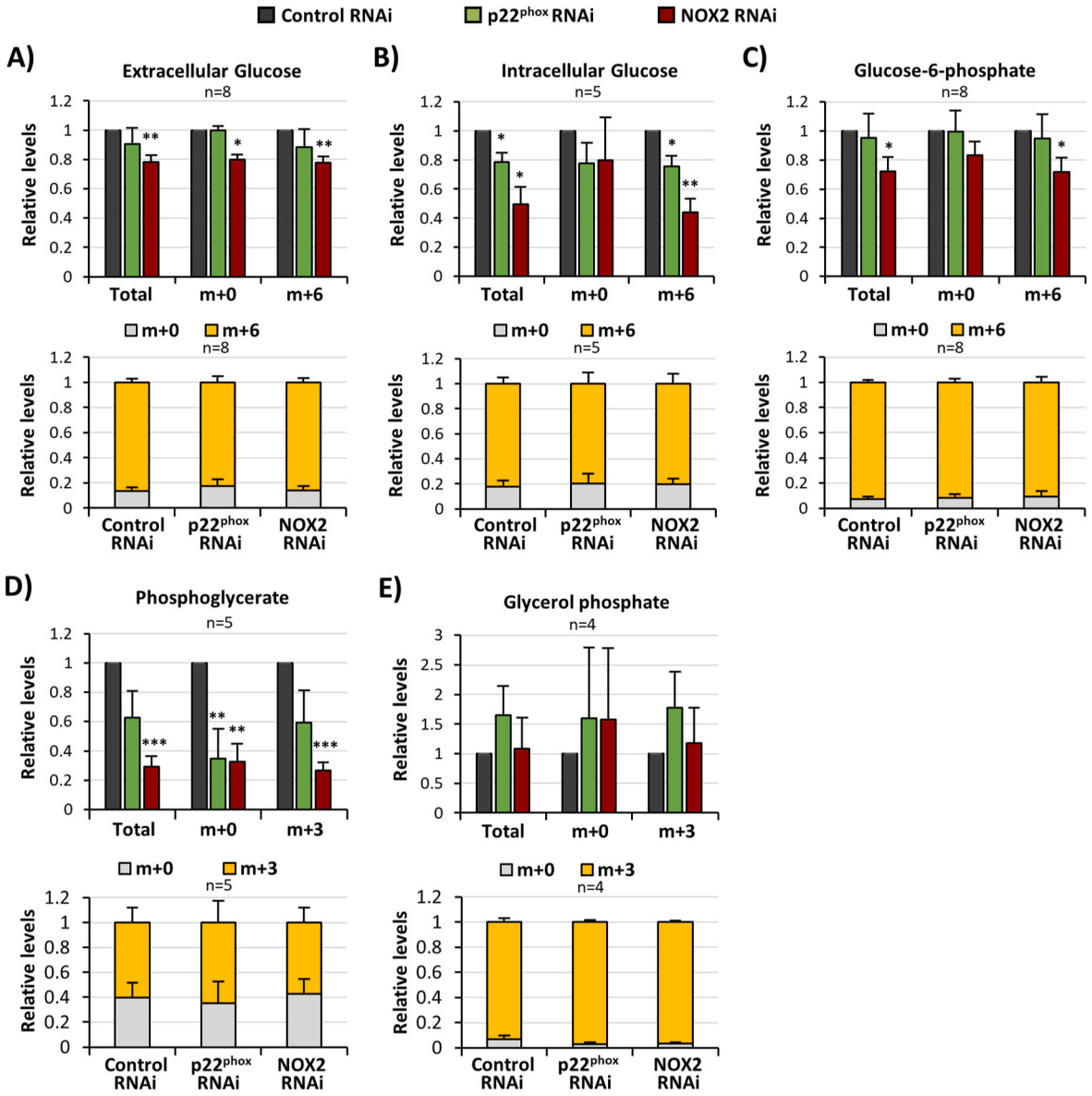

Fig. 1. NOX2, but not p22^{phox} silencing, induces the flow of glucose through glycolysis in K562 cells. Metabolite levels were analysed by HPLC after 2 h of culture in medium containing 2 g/L$^{13}C_6$-glucose. **(A–E)** The graphs at the top show the relative levels of (A) extracellular glucose, (B) intracellular glucose, (C) glucose-6-phosphate, (D) phosphoglycerate and (E) glycerol phosphate labelled with ^{13}C (m + n), without ^{13}C (m+0) and total, normalized to protein concentration; bottom panel show the relative proportion of both fractions for each metabolite. Data show mean ± SE (standard error). * denotes significant differences with respect to control cells (two-way Student's T-Test). HPLC, high performance liquid chromatography.

suggest that NOX2-silenced cells uptake and use glucose faster than control cells.

We noticed that while the percentage of ^{13}C-labelled-glucose or ^{13}C-labelled-phosphoglucose was above 80% (Fig. 1B–C, bottom panels), this percentage dropped to 60% in the case of phosphoglycerate (Fig. 1D, bottom panel). This might be due to the diversion of glucose towards alternative metabolic destinies, such the pentose phosphate pathway (PPP). However, no differences were found in several PPP intermediates (Supplementary Figs. 2B–D), whose percentage of ^{13}C-labelling only reached about 50%, suggesting that the flow of glucose through the PPP is not favoured over the glycolysis. The global level of NADPH, one of the main products of the PPP pathway, and the NADP$^+$/NADPH ratio tended to be diminished upon NOX2 silencing, although not reaching statistical significance (Supplementary Fig. 2E).

An alternative possibility would be the diversion of glucose to lipid anabolism through the conversion of dihydroxyacetone phosphate to glycerol phosphate. Although no differences were detected regarding the levels of glycerol phosphate, we noticed that virtually all this metabolite was ^{13}C-labelled, especially in the NOX2-silenced cells (Fig. 1E, bottom panel). This is consistent with the notion that these cells divert a significant part of glucose carbon towards the formation of glycerol phosphate.

Regarding p22^{phox}-silenced cells, we only observed a slight decrease in the concentration of intracellular free glucose, but the other metabolites were not affected (Fig. 1).

In agreement with increased glycolysis; silencing of NOX2 promoted lactate dehydrogenase (LDH) activity, which was phenocopied in p22^{phox}-silenced cells (Fig. 2A). Moreover, NOX2-silenced cells showed a faster acidification of the extracellular medium (data not shown), what we surmised that could be due to lactate secretion. However, when we measured the levels of this metabolite intracellularly (Fig. 2B) and extracellularly (Fig. 2C), there were no differences between NOX2-silenced and control cells. The lower proportion of ^{13}C-labelled phosphoglycerate is also reflected in a reduced proportion of ^{13}C-labelled lactate, which drops to 50–60% at the intracellular level (Fig. 2B, bottom panel) and a mere 30% in extracellular lactate (Fig. 2C, bottom panel). In addition, intracellular ^{13}C-labelled lactate ratio in NOX2-silenced cells resulted higher than in control cells (Fig. 2B, bottom

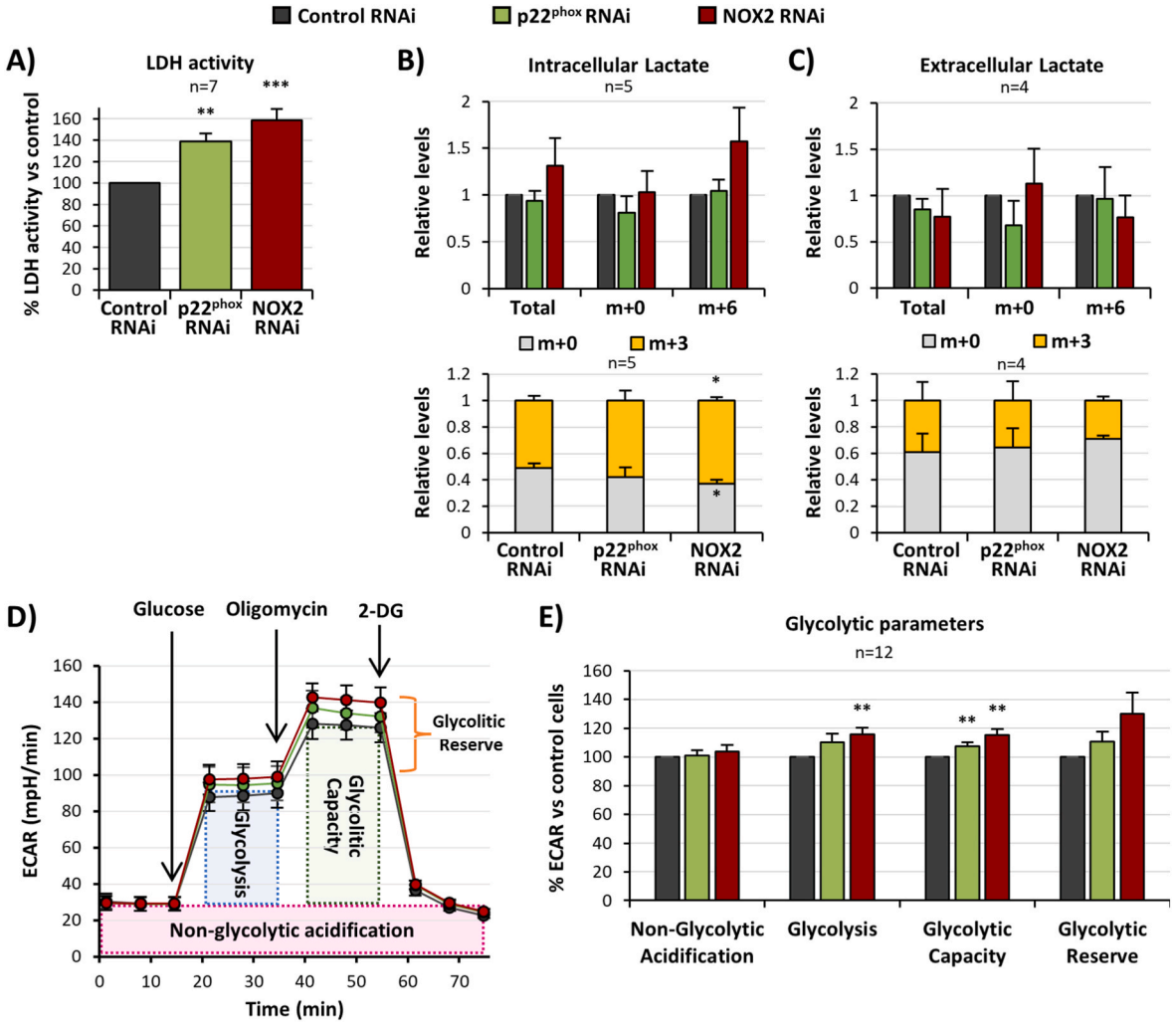

Fig. 2. NOX2 induces glycolysis and LDH activity without affecting lactate levels. Metabolism parameters were analysed in NOX2-, p22^{phox}-silenced and control K562 cells. **(A)** Relative LDH activity normalised with respect to control cells. **(B–C)** Relative levels of intracellular (B) and extracellular (C) lactate analysed after 2 h of culture in medium containing 2 g/L $^{13}C_6$-glucose by HPLC. The graphs at the top show relative levels of lactate labelled with ^{13}C (m+6), without ^{13}C (m+0) and total, normalized to protein concentration; bottom panel show the relative proportion of both fractions. **(D)** ECAR profile (n = 12) and **(E)** ECAR percentage of glycolytic parameters analysed using the Agilent "*Glyco Stress Test*". Experiments were performed on 25,000 cells/well. 10 mM Glucose, 1.5 μM oligomycin and 50 mM 2-DG were sequentially injected at the times specified in the graph. Data are shown as the mean ± SE. * represents significant differences with respect to control cells (two-way Student's T-Test). LDH, lactate dehydrogenase; HPLC, high performance liquid chromatography; ECAR, extracellular acidification rate; 2-DG, 2-Deoxy-D-glucose.

panel), while the relation is the opposite when we look at the extracellular ^{13}C-labelled lactate (Fig. 2C, bottom panel). This could indicate that the flow of glucose towards lactate is not favoured, and only a minor proportion is secreted. All in all, this suggest that these cells, especially NOX2-silenced cells, use lactate as a carbon building block rather than excreting it out.

The results described so far allow us to suggest that NOX2-silenced cells display a faster metabolism of glucose than control cells. To test this further, we use Seahorse technology from Agilent in order to analyse the bioenergetics metabolism, aerobic glycolysis and mitochondrial oxidative phosphorylation, in real time. First, using a *Seahorse XF Glycolysis Stress Test* we found that NOX2-silenced cells displayed higher extracellular acidification rates (ECAR) compared to control cells (Fig. 2D). In fact, the parameter analysis revealed a significantly enhanced *Glycolysis* and *Glycolytic capacity* in NOX2-silenced cells (Fig. 2E), which is consistent with a faster use of glucose through the glycolytic pathway by these cells, as suggested above. p22^{phox}-silenced cells showed a similar trend, which was only significant on *glycolytic capacity* (Fig. 2D–E).

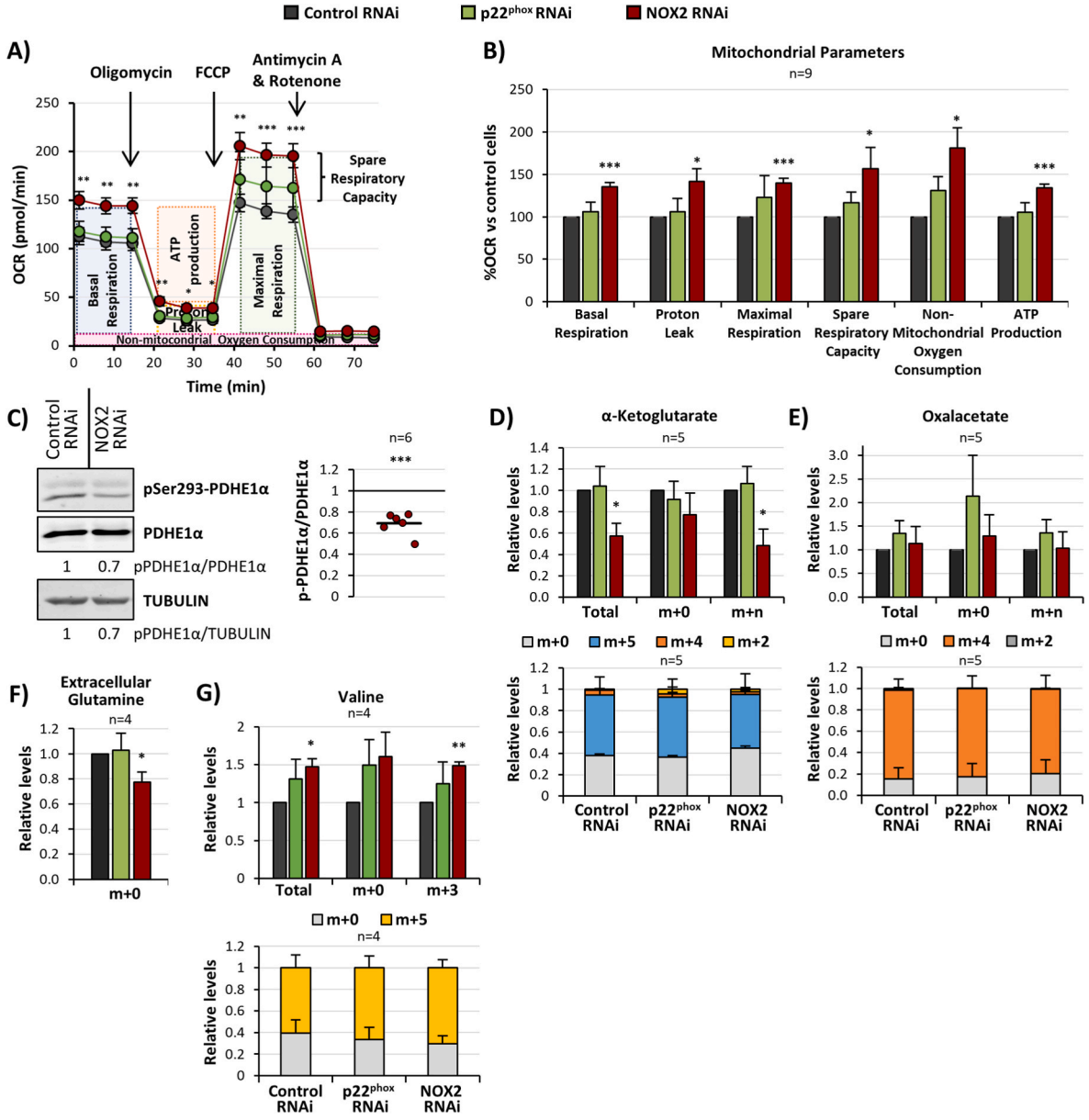

Fig. 3. NOX2 knockdown increases respiration and nutrient input to mitochondria in K562 cells. (A) OCR of cells stably silenced against p22^{phox} and NOX2 and control cells, showing injections and phases obtained following Agilent's "*Mito stress*" protocol (n = 9). **(B)** OCR percentage of the parameters obtained following the "*Mito stress*" protocol. The experiments were performed on 50,000 cells/well. 1.5 μM Oligomycin, 0.9 μM FCCP and 0.5 μM rotenone/antimycin were sequentially injected at the times specified in the graph. **(C)** Phosphorylation of PDHE1α (Ser-293) analysed by immunoblotting in NOX2-silenced and control cells (n = 6). A representative image, of phospho-PDHE1α (Ser-293) and PDHE1α using TUBULIN as a loading control is shown on the left. Right graph shows phospho-PDHE1α (Ser-293)/PDHE1α protein ratio respect to control cells where each point represents one experiment. **(D–G)** Relative levels of α-ketoglutarate (D), oxalacetate (E), glutamine (F) and valine (G) analysed after 2 h of culture in medium containing 2 g/L $^{13}C_6$-glucose by HPLC. The graphs at the top show relative levels of each metabolite labelled with ^{13}C (m + n), without ^{13}C (m+0) and total, normalized to protein concentration; and D, E and G bottom panel show the relative ratio of labelled to unlabelled metabolite. Data show mean ± SE. * represents significant differences with respect to control cells (two-way Student's T-Test). OCR, oxygen consumption rate; FCCP, carbonyl cyanide 4-(trifluoromethoxy) phenylhydrazone; PDHE1α, pyruvate dehydrogenase E1 component; HPLC, high performance liquid chromatography.

3.2. Silencing of NOX2 enhances mitochondrial respiration

NOX2-silenced cells displayed a high glycolytic rate (Fig. 2E), which however was not associated to the production and secretion of lactate. Despite that, these cells showed a fast acidification of the extracellular medium. If the extracellular acidification was not caused by lactate secretion, we wondered whether it could be consequence of a higher mitochondrial respiration leading to a higher production of CO_2 and therefore CO_3H_2. To test this possibility, we analysed mitochondrial respiration by using a *Seahorse XF Cell Mito Stress*.

We found that the profile of oxygen consumption rate (OCR) was significantly enhanced in NOX2-silenced cells along the whole assay (Fig. 3A), supporting a higher mitochondrial respiratory efficiency, as corroborated by the significant increase in all the parameters analysed (Fig. 3B). These results were corroborated with a second RNAi sequence against NOX2 (Supplementary Fig. 3A). In consonance with the ECAR data, $p22^{phox}$-silenced cells showed a trend of OCR increase, but no significant differences were found in any of the respiration parameters analysed (Fig. 3A–B).

A higher OCR must be matched by an enhanced entry of fuel into the TCA cycle. Pyruvate coming from glycolysis must be transformed into acetyl-CoA by the Pyruvate dehydrogenase complex (PDC). Therefore, if glucose entry into the TCA cycle is enhanced, PDC should be more active. PDC activity is subjected to allosteric and covalent regulation; phosphorylation of pyruvate dehydrogenase E1α subunit (PDHE1α) at several serine residues inhibits enzyme activity [11]. Consistent with a higher PDC activity, phosphorylation of E1α Ser-293 was decreased in NOX2-silenced cells (Fig. 3C). After 2 h of culture with D-glucose-$^{13}C_6$ we could detect the TCA cycle intermediates oxaloacetate (OAA) and α-ketoglutarate (α-KG), that as happened for glycolytic intermediates, were highly ^{13}C-labelled (Fig. 3D–E). This, together with the increased PDC activity suggest that the flow of glucose towards anaplerosis of intermediates of the TCA cycle is favoured in NOX2-silenced cells. Nevertheless, we noticed that while more than 80% of OAA was ^{13}C-labelled, the percentage in the case of α-KG was only around 60% (Fig. 3D–E, bottom panel). Such difference could be explained by the synthesis of α-KG from other suitable TCA cycle intermediates, such as glutamine, that was not ^{13}C-labelled in our experiments. In agreement with this hypothesis there was a significant reduction of extracellular glutamine in NOX2-silenced cells (Fig. 3F), and these cells showed the lowest proportion of ^{13}C-labelled α-KG (Fig. 3D, bottom panel). Therefore, NOX2-silenced cells also showed an enhanced entry of glutamine in the TCA cycle.

No differences were observed regarding OAA levels, but in NOX2-silenced cells there was a significant decrease of α-KG (Fig. 3D). This might seem initially contradictory with a higher conversion of glutamine into α-KG, but it could be explained by the diversion of α-KG towards amino acids synthesis, and the use of glutamine as a source of nitrogen. In agreement with this idea, we found a significant increase of valine, that was at the same time highly ^{13}C-labelled, in NOX2-silenced cells (Fig. 3G).

3.3. Silencing of NOX2 alters mitochondrial parameters revealing mitochondrial dysfunction

The results presented so far, suggest that NOX2 silencing enhanced the rate of glycolytic and mitochondrial metabolism. However, these cells proliferated less compared to RNAi control cells either in the presence of glucose or galactose, the later relying on mitochondrial metabolism (Supplementary Fig. 3B). These changes cannot be explained by an alteration in the expression of glucose and galactose transporters levels upon NOX2 silencing (SRA database, PRJNA928236).

Therefore, although NOX2 silencing seems to increase the rate of metabolism, such metabolism is less efficient, especially when mitochondria are required as the galactose experiments point out, suggesting mitochondria malfunction upon NOX2 silencing. To test this hypothesis, we analyse several mitochondrial parameters, including mitochondrial ROS, mitochondria number, and the protein levels of several subunits of the mitochondrial respiratory chain complexes (RCC).

We observed an increase in mitochondrial ROS levels in NOX2-silenced cells (Fig. 4A), suggesting that these cells were subjected to a higher mitochondrial stress. These cells also showed a slight increase in MitoTracker staining (Fig. 4B), which could be explained by an increase in mitochondrial mass.

Mitochondrial DNA (mtDNA) codes for 13 proteins and 2 rRNA required for mitochondrial structure and function. Unlike nuclear DNA (nDNA) the number of copies of mtDNA (mtDNA CN) can go from 100 to 10,000. The ratio mtDNA/nDNA is used as an indicator of mitochondrial biogenesis and at the same time, can be used as a good biomarker of mitochondrial health [27]. Our results showed a reduction of this ratio in NOX2-silenced cells after 2 days of culture (Fig. 4C), suggesting a reduction of mtDNA CN as the cells consume the nutrients. Among the factors that have been involved in a reduction of mtDNA CN, an enhanced mitochondrial oxidative stress has been postulated [35]. Along this line NOX2-silenced cells presented a higher level of mitochondrial ROS (Fig. 4A), which might be related with the alteration of mtDNA CN.

To understand whether the lower mtDNA CN was accompanied by a decrease in RCCs, we studied the protein levels of crucial subunits of the different RCCs. Western blot analysis and immunodetection with the OXPHOS antibody cocktail recognizing NDUFB8 (Complex I), SDHB (Complex II), UQCRC2 (Complex III), MTCO1 (Complex IV) and ATP5A (Complex V) evidenced a decrease in all the proteins except SDHB, the only one exclusively nuclear-encoded (Complex II) [36] (Fig. 4D).

3.4. Signalling pathways downstream of BCR-ABL are altered by NOX2 silencing

As we described previously, NADPH oxidases knockdown reduced BCR-ABL activation and some of its downstream pathways [17]. With this in mind, we analysed the state of activation of some signalling pathways downstream of BCR-ABL that are important for metabolism regulation. Most of the metabolic changes associated to BCR-ABL expression have been related with the activation of the phosphatidylinositol 3-kinase (PI3K)/AKT/mammalian target of rapamycin (mTOR) signalling pathway [16]. Besides, this pathway is essential for cell survival, proliferation, and differentiation [37]. The effect of NOX2 silencing on the activity of this signalling pathway was dependent on the days of culture. On day 1 we observed a decrease of AKT activation (Fig. 5A), which was corroborated by a decreased phosphorylation of its substrates (Fig. 5B). This is consistent with the decreased activation of mTOR and ribosomal protein S6 kinase (p70S6K) (Fig. 5A). However, on day 2 of culture, with exception of mTOR inactivation, these changes were reverted (Fig. 5A and B), suggesting a reactivation of this pathway, probably due to fuel starving.

The permanent inactivation of mTOR could be due to the influence of other signalling pathways different from the PI3K pathway. It has been described that BCR-ABL induces a strong activation of phospholipase C gamma 1 (PLCγ1), which leads to the AKT-independent activation of mTOR [38]. NOX2-silenced cells showed a lower activation of PLCγ1 (Fig. 5C), which could contribute to the lower activation of mTOR.

As pointed above, ROS levels can regulate the activity of several master regulators of metabolism such as adenosine monophosphate-activated protein kinase (AMPK), Hypoxia-inducible factor 1 (HIF-1), Nuclear factor E2-related factor 2 (NRF2) or ataxia-telangiectasia mutated (ATM) protein kinase [2]. AMPK promotes glycolysis, fatty acid oxidation and mitochondrial biogenesis [39]. Acetyl-CoA carboxylase (ACC) is directly phosphorylated and inactivated by AMPK. We detected an increase of ACC phosphorylation on Ser-9 in NOX2-silenced cells (Fig. 5D). Moreover, mTOR can be inactivated by AMPK [40]. The lower activation state of mTOR (Fig. 5A) and ACC (Fig. 5D) are

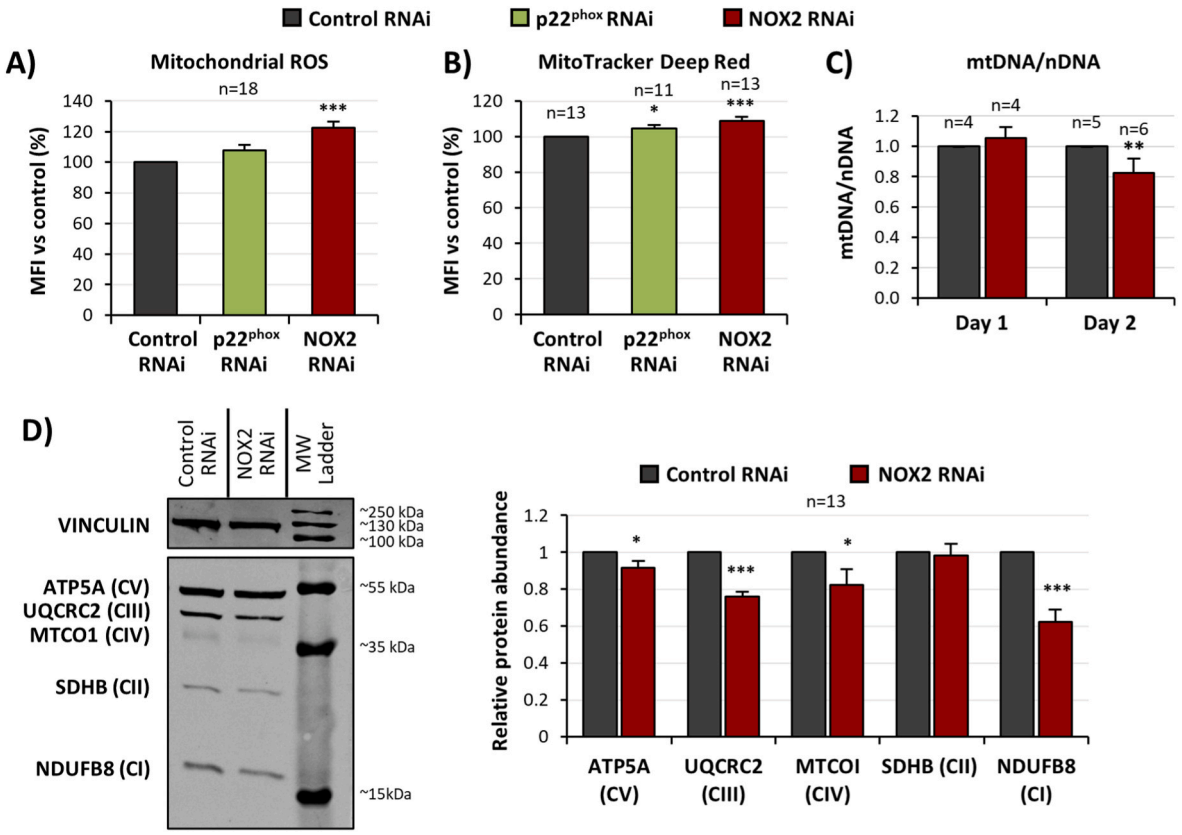

Fig. 4. Mitochondrial parameters of NOX2-silenced cells reveal mitochondrial dysfunction. (A–B) Bars graphs show MFI percentage of mitochondrial ROS analysed by labelling with 5 μM MitoSOX (A) and mitochondrial content analysed by labelling with 200 nM MitoTracker Deep Red (B). **(C)** mtDNA/nDNA ratio of NOX2-and p22^{phox}-silenced cells relative to control cells after one or two days of culture in RPMI complete medium. **(D)** Representative Western Blot image (left) and relative protein abundance quantification of "n" biological replicates (right) of ATP5A, UQCRC2, MTCO1, SDHB and NDUFB8 proteins detected in total protein lysates from control and NOX2-silenced K562 cells. Data are shown as mean ± SE. * Reflect significant differences versus control cells (two-way Student's T-Test). MFI, mean fluorescence intensity; mtDNA/nDNA ratio; mitochondrial DNA/nuclear DNA ratio; ATP5A, ATP synthase 5 subunit alpha; UQCRC2, ubiquinol-cytochrome C reductase core protein 2; MTCO1, mitochondrially encoded cytochrome C oxidase I; SDHB, succinate dehydrogenase B; NDUFB8, NADH:Ubiquinone oxidoreductase subunit B8. (For interpretation of the references to colour in this figure legend, the reader is referred to the Web version of this article.)

consistent with an enhanced activity of AMPK upon NOX2 silencing, which would agree with the metabolic alterations described above.

Another master regulator of metabolism such glycogen synthase kinase-3 beta (GSK3β) can be downstream of PI3K/AKT. GSK3β phosphorylation on Ser-9 by AKT leads to inhibition [41]. NOX2 silencing reduced GSK3β phosphorylation on Ser-9, reflecting a higher activity of this enzyme (Fig. 5E). NRF2 protein stability is controlled by a number of signalling pathways, including the PI3K/AKT/GSK3β pathway [42]. NRF2 levels were slightly decreased in NOX2-silenced cells on day 1 of culture, and they recovered on day 2 (Supplementary Fig. 5B). The early NRF2 downregulation could be due to the GSK3β activation.

3.5. Silencing of NOX2 enhances NOX4 expression

Giving that NOX2 is the main isoform in hematopoietic cells [43] we expected that NOX2 and p22^{phox} silencing would produce a similar phenotype. However, this was not the case, as it can be observed in the figures above. Therefore, we hypothesised that such differences could be explained by the intervention of an additional p22^{phox}-dependent NADPH oxidase in the control of CML cells metabolism. In this respect, NOX4 seemed a suitable candidate; its expression in the mitochondria has been described [44], NOX4 behaves as a mitochondrial sensor [23], and intervenes in mitochondrial dynamics [24]. We have previously observed that downregulation of NOX2 in hematopoietic cells led to an increase of *NOX4* mRNA levels (our unpublished data). In fact, it has been described that mutual regulation may exist between both isoforms in skeletal muscle [45], macrophages [46], lung endothelial cells [47], cardiovascular system [48] or hepatocellular carcinoma [49]. In agreement with these antecedents, we found an upregulation of *NOX4* mRNA in NOX2-silenced cells (Fig. 6A). In addition, we detected an increase of NOX4 (Fig. 6B) and p22^{phox} (Fig. 6C) protein levels in the mitochondrial fraction of NOX2-silenced cells. These results are consistent with the notion that NOX2 silencing induces the stabilization of NOX4 in the mitochondria. In agreement with this, a recent report shows that inactivation of Nox2 complex induces an enhancenment of both Nox4 and p22^{phox} protein levels [45].

Given the relevance of NADPH oxidase driven ROS production for the BCR-ABL signaling [17], we wondered whether *NOX4* expression could be under the control of BCR-ABL. Our results show that BCR-ABL inhibition led to an increase in *NOX4* mRNA expression (Fig. 6D), as it happened upon NOX2 silencing (Fig. 6A). This results are consistent with the notion that *NOX4* expression is governed by BCR-ABL/NOX2 signalling. An interesting issue for the future will be to identify the transcription factors regulating *NOX4* expression in CML. To get some insight in this issue, we analysed the expression of almost fifty different transcription factors that have been previously related in the regulation of *NOX4* transcription in NOX2-silenced cells. Among them HIF1α [50], small mother against decapentaplegic 1 (SMAD1) and 6 (SMAD6) [51], Sp1 and Sp3 [52] showed a trend of increase in NOX2-silenced cells (Supplementary Table III).

Given the multiple reports linking NOX4 and mitochondrial function [23,24,44,53], we wondered whether the alterations in mitochondrial metabolism observed upon NOX2 silencing could be related to NOX4 upregulation. NOX4-silenced cells tended to have a lower OCR profile

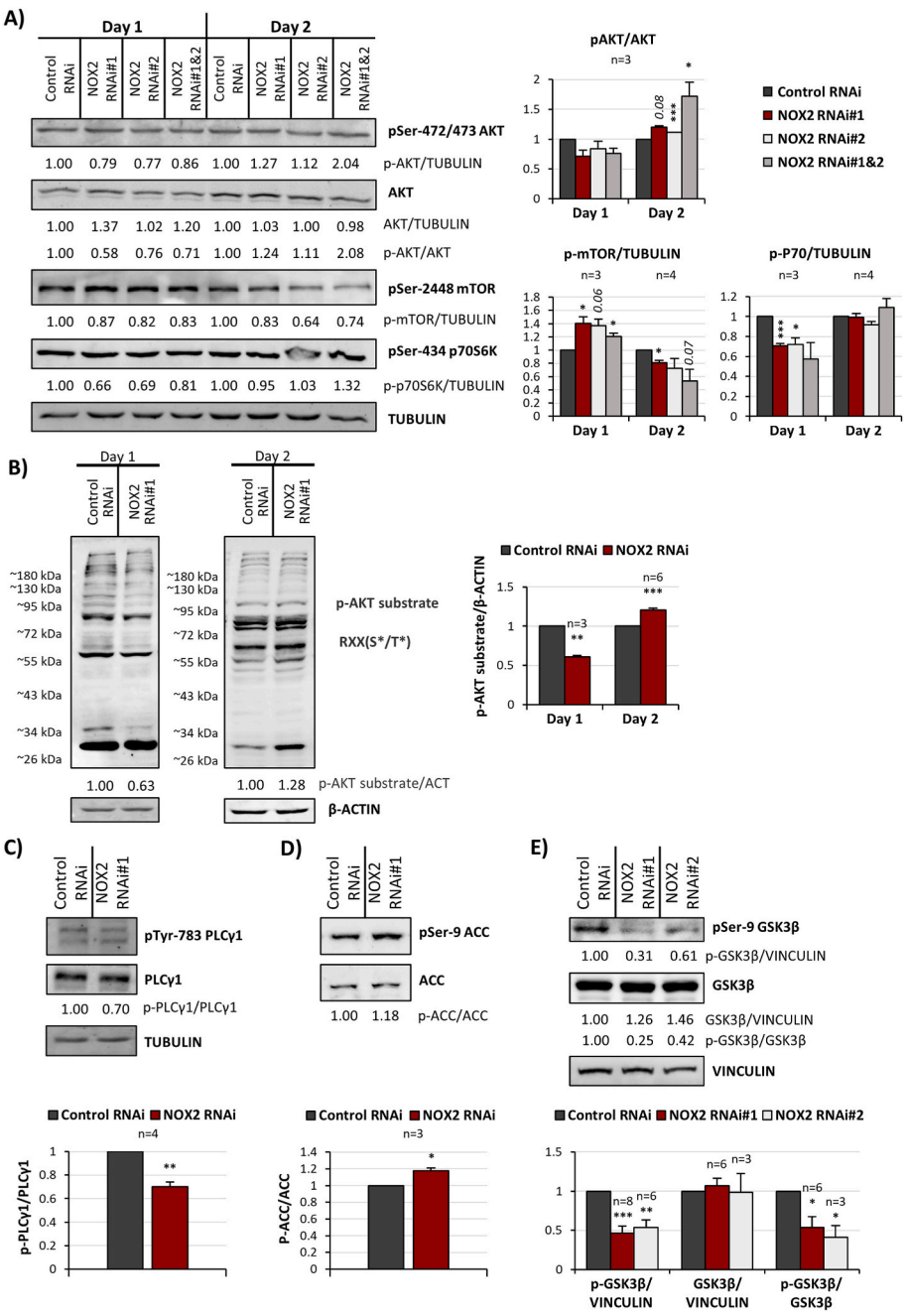

Fig. 5. NOX2 silencing induces lower mTOR activation along with increased GSK3β activation. The levels of signalling proteins in control and NOX2-silenced K562 cells were analysed by immunoblotting in whole cell extracts. **(A)** Analysis of the PI3K/AKT/mTOR pathway after one or two days of culture in RPMI complete medium. Left image shows a representative Western Blot imagen of PI3K/AKT/mTOR pathway and right graphs show the quantification of "n" biological replicates. **(B)** Western Blot images of phospho-AKT substrate (RXXS*/T*) normalized by β-ACTIN after one or two days of culture in RPMI complete medium (left) and quantification of "n" biological replicates (right). **(C)** Western Blot image of phopho-PLCγ1 (Tyr-783) and PLCγ1. Quantification and biological replicates (n) are shown at the bottom panel. **(D)** Western Blot image of phospho-ACC (Ser-9) and ACC. Quantification and biological replicates (n) are shown at the bottom panel. **(E)** Western Blot image of phospho-GSK3β (Ser-9) and GSK3β. Quantification and biological replicates (n) are shown at the bottom panel. Bar graphs show mean ± SE. * represents significant differences with respect to control cells (two-way Student's T-Test). PI3K, fosfatidilinositol-3-kinasa; AKT, protein kinase B; mTOR, mammalian target of rapamycin; PLCγ1, phospholipase C gamma 1; ACC, acetyl-CoA carboxylase; GSK3β, glycogen synthase kinase-3 beta.

(Fig. 6E), reflected in the significant reduction in the *Maximal* and *Spare respiratory capacities*, and in the *ATP production* (Fig. 6F). This adds to previous works relating NOX4 to mitochondrial metabolism. Moreover, when we silenced NOX4 in the previously NOX2-silenced cells, the increase in all mitochondrial metabolism parameters induced by NOX2 silencing was prevented, even leading to a further decrease (Fig. 6E–F). Along the same line, we observed an enhanced phosphorylation of PDHE1α Ser-293 upon NOX4 silencing, reflecting a lower PDC activity (Fig. 6G). Because of these metabolic alterations, NOX4-and the doubly NOX2/NOX4-silenced cells proliferated less than control cells, either in the presence of glucose or galactose (Supplementary Fig. 3B).

As mentioned above, mitochondrial ROS levels in NOX2-silenced cells were increased (Fig. 4A), which was reverted in the doubly NOX2/NOX4-silenced cells (Fig. 6H). This strongly suggests that the mitochondrial oxidative stress in NOX2-silenced cells is caused by NOX4 overexpression.

These results allow us to propose that the enhancement of mitochondrial metabolism induced by NOX2 silencing is due to NOX4 upregulation, suggesting the existence of a potential NOX2-NOX4-mitochondria functional axis in CML cells.

The OCR data presented above have been obtained in whole cells, therefore, the alteration of mitochondrial metabolism observed upon NOX2 and NOX4 silencing could be explained either by extrinsic factors such upstream signalling events or differences in nutrient availability, or by an intrinsic alteration of mitochondria.

To sort out these possibilities, we analysed mitochondrial function after organelle isolation by using a Clark's type oxygen electrode to measure O_2 consumption in presence of complex I substrates in a KCl-containing medium [54]. Oxygen consumption was measured after addition of ADP (State 3) to record maximal coupled respiratory capacity, followed by oligomycin (State 4) to exclude the contribution of the ATP synthase, and the State3/State4 ratio (RCR, respiratory control

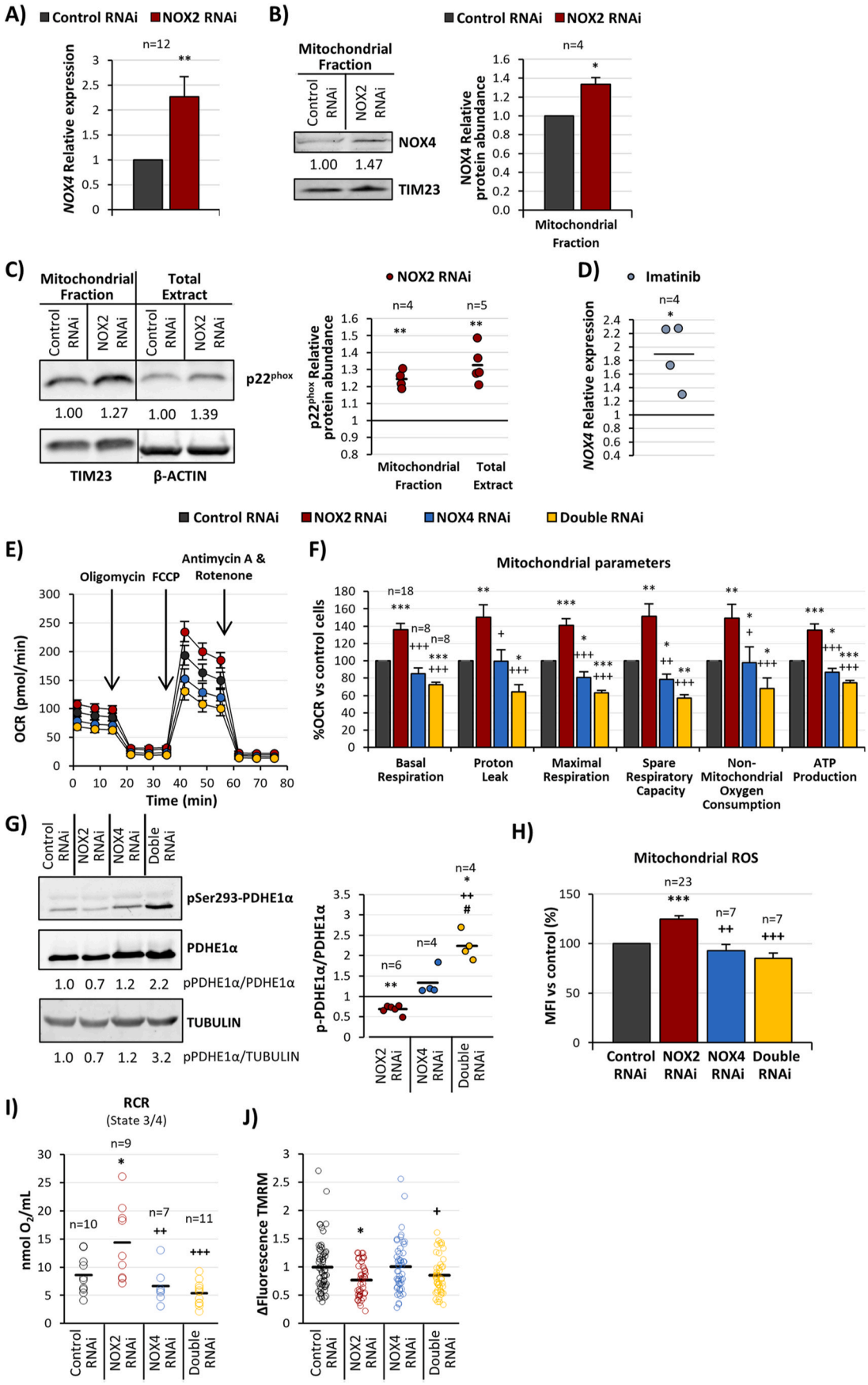

(caption on next page)

Fig. 6. NOX2 silencing induces an increase in NOX4 expression and NOX2/4 double silencing reverses NOX2-induced OXPHOS increase. (A) Relative expression of *NOX4* mRNA in control and NOX2-silenced K562 cells (mean ± SE). **(B)** Representative Western Blot image of NOX4 abundance in mitochondria-enriched fraction in control and NOX2-silenced K562 cells normalized by TIM23 (left panel). Quantification and biological replicates (n) are shown on the right bar graph panel (mean ± SE). **(C)** Representative Western Blot image of $p22^{phox}$ protein abundance in the mitochondria-enriched fraction normalized by TIM23, and in total extracts normalized by β-ACTIN (left panel). Quantification and (n) are shown on the right graph panel, where each point represents one biological replicate, **(D)** Relative expression of *NOX4* mRNA in K562 cell line treated for 6 h with 0,2 μM imatinib. Each point represents one independent biological replicate. **(E–F)** Analysis in whole cells of NOX2, NOX4 and NOX2/NOX4 double silencing effect on (E) OCR profile and (F) % OCR of mitochondrial parameters using Agilent's mitochondrial stress test ("*Mito stress test*"). Experiments were performed on 50,000 cells/well. 1.5 μM Oligomycin, 0.9 μM FCCP and 0.5 μM rotenone/antimycin were sequentially injected at the times specified in the graph. Bar graphs show mean ± SE. **(G)** Phosphorylation of PDHE1α (Ser-293) analysed by immunoblotting in NOX2-, NOX4-, NOX2/NOX4-silenced and control cells. Left image panel shows a representative Western Blot of phospho-PDHE1α (Ser-293) and PDHE1α using TUBULIN as a loading control. Right graph shows phospho-PDHE1α (Ser-293)/PDHE1α protein ratio respect to control cells where each point represents one independent biological replicate (n). **(H)** Bars graphs show MFI percentage of mitochondrial ROS analysed by labelling with 5 μM MitoSOX. Data are shown as mean ± SE. **(I)** Analysis of RCR in isolated mitochondria by oxygraphy in K562 cells silenced for NOX2 and/or NOX4. Each point represents one technical replicate of 5 biological replicates. **(J)** Mitochondrial membrane potential was monitored by using TMRM and calculating the delta fluorescence (ΔFluorescence) value after complete depolarization with FCCP. Data are shown as ΔFluorescence TMRM normalized to the control siRNA mean. Each point represents the ΔFluorescence of one cell from 5 biological replicates. * Reflect significant differences versus control cells, + versus NOX2-silenced cells and # versus NOX4-silenced cells. For panel A–D two-way Student's T-Test was applicated, for F-J two-way ANOVA test was used. Double RNAi, NOX2/NOX4-silenced cells; OXPHOS, oxidative phosphorylation; TIM23, translocase of the inner mitochondrial membrane 23; OCR, oxygen consumption rate; FCCP, carbonyl cyanide 4-(trifluoromethoxy) phenylhydrazone; PDHE1α, pyruvate dehydrogenase E1 component; RCR, respiratory control rate; TMRM, tetramethylrhodamine methyl ester.

rate) has been calculated as a fair indicator of mitochondrial functionality. In line with the OCR experiments (Fig. 6E–F), NOX2-silenced mitochondria display a higher RCR than NOX4-silenced mitochondria (Fig. 6I). More importantly, NOX4 silencing reverts the increase of RCR mediated by NOX2 silencing in the doubly silenced cells (Fig. 6I), suggesting that, indeed, NOX2 is epistatic to NOX4 in the regulation of mitochondrial respiration.

The alteration of mitochondrial membrane potential (ΔΨm) is a good indicator of mitochondrial health. NOX2-silenced cells showed a lower ΔΨm than control cells (Fig. 6J), which is in agreement with the enhanced proton leak observed in these cells (Fig. 6F). This adds to the results reported above suggesting mitochondrial malfunction (Fig. 4). Although no differences in ΔΨm were found between NOX4-silenced and control cells, NOX4 silencing reverted the decreased ΔΨm induced by NOX2 silencing in the doubly silenced cells (Fig. 6J). This further supports the functional connection NOX2-NOX4.

3.6. NOX2 and NOX4 silencing alter mitochondria size and number

Since alterations in mitochondria ultrastructure and morphology mirrors their function, we analysed these parameters by confocal microscopy and transmission electron microscopy (TEM). The absence of NOX2, NOX4, or both does not significantly impact the phenotype of the mitochondrial network. Indeed, a similar elongated and interconnected network is observed in all four cellular phenotypes (Supplementary Figs. 3C–D). Still, whether this phenotype could be more sensitive to changes under specific stress conditions requires further studies. Although the cristae shape did not change between the different cell lines (Supplementary Fig. 3E), the number of mitochondria per cell was slightly higher in NOX2-silenced cells (Fig. 7A) with respect to the control, showing both an equivalent mitochondrial area (Fig. 7B). NOX4-silenced cells showed a significantly higher mitochondrial density than in control cells (Fig. 7A), that was accompanied by a decrease in their size (Fig. 7B). Noteworthy, the latter phenotype can be found in mitophagy-related conditions, where dysfunctional mitochondria are eliminated to favour cell viability [55,56]. Surprisingly, the phenotype described in NOX4-silenced cells was rescued in the doubly silenced cells, displaying a lower mitochondria number comparable to the control condition. Consistent with the concept that changes in mitochondrial size might result from unbalanced fusion and fission event, we observed a decrease in the protein levels of the profusion protein MFN2 in whole cell extracts and mitochondrial fraction from NOX2-and

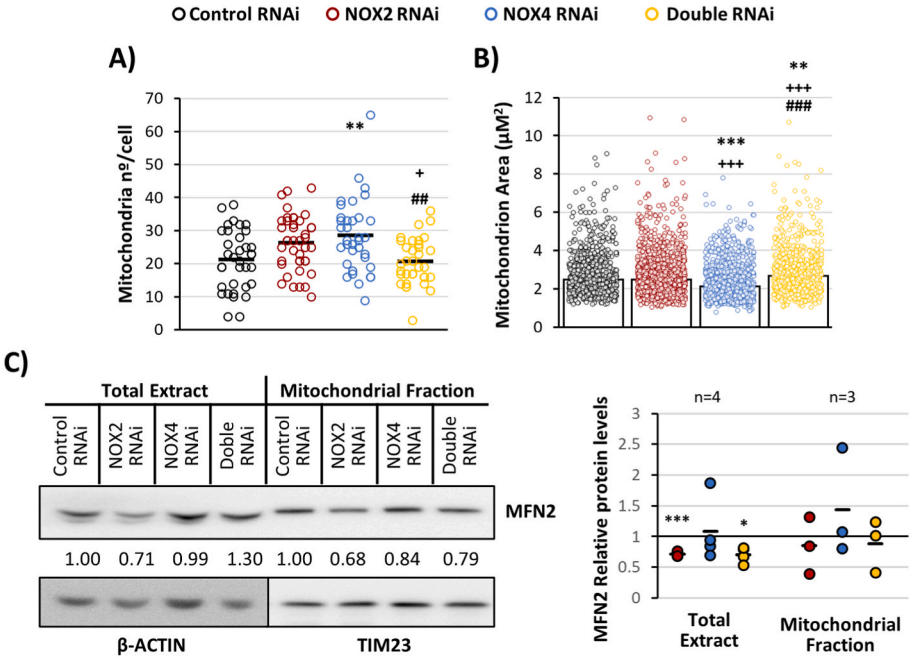

Fig. 7. NOX2-NOX4 axis affects mitochondrial size, number and dynamics. The number of mitochondrion per cell and their area was monitored by TEM as described in the methods section in control, NOX2-, NOX4-and NOX2/NOX4-doubly silenced K562 cells. **(A)** Number of mitochondria per cell. **(B)** Mitochondrion area. **(C)** MFN2 protein expression in whole cells extracts and in mitochondrial enriched fraction. The fraction enriched in mitochondria was normalized with TIM23 and whole cells extracts with β-ACTIN. Representative Western Blot image (left) and relative protein abundance with respect to control cells (line with value 1) are shown (right). Each point represents one biological replicate and the horizontal line the mean of MFN2 levels within each cell line. * Reflect significant differences versus control cells, + versus NOX2-silenced cells and # versus NOX4-silenced cells (two-way ANOVA). Double RNAi, NOX2/NOX4-silenced cells. TEM, transmission electron microscopy; MFN2, mitofusin 2; TIM23, translocase of the inner mitochondrial membrane 23.

NOX2/NOX4 double-silenced cells (Fig. 7C).

3.7. NOX2 and NOX4 silencing enhances mitochondrial calcium level

Mitochondria function highly depends on Ca^{2+} signalling, that enters from the endoplasmic reticulum (ER) through mitochondria-endoplasmic reticulum contacts (MERCs) [57]. MERCs are very dynamic structures that respond to metabolic changes, and regulate important processes such as lipid traffic, mitochondrial fusion/fission, autophagy, apoptosis or Ca^{2+} transfer [57]. Interestingly, the number of MERCs in NOX2-and NOX4-silenced cells doubled that quantified in control cells, while the cells simultaneously silenced for both NOXs showed a number of MERCs equivalent to the control cells (Fig. 8A). This result raises the possibility of an alteration of mitochondrial Ca^{2+} ($mtCa^{2+}$) levels. Indeed, the concentration of basal $mtCa^{2+}$ was significantly higher in all silenced cells (Fig. 8B).

The transfer of Ca^{2+} from the ER to the mitochondria can be triggered by the activation of the inositol 1,4,5-trisphosphate receptor (IP3R) by upstream signalling, such for instance the activation of P2Y receptors by ATP. Control cells responded to 100 μM ATP stimulation, with the expected increase in $mtCa^{2+}$ (Supplementary Fig. 4A), while none of the silenced cells responded to ATP.

Finally, we analysed the effect of the activation of store operated calcium entry (SOCE) on the mitochondrial Ca^{2+} (Supplementary Fig. 4B). Even after thapsigargin-induced ER emptying in calcium-free medium the $[Ca^{2+}]_M$ was higher in NOX2-silenced cells (Fig. 8C). After SOCE activation, NOX2-silenced cells showed a faster $mtCa^{2+}$ uptake (Fig. 8D). Therefore, it seems that NOX2-silenced cells show a higher capacity of mitochondrial calcium uptake via SOCE, which could also contribute to the higher basal $mtCa^{2+}$ found in these cells (Fig. 8B and C).

3.8. NOX2 and NOX4 silencing alters the transcriptomic profile of genes involved in metabolism

The results presented so far suggest the existence of a functional axis NOX2-NOX4-mitochondria. It is reasonable to think that gene expression regulation would be one of the main means to control metabolism. To test that, we performed RNAseq transcriptomic analyses (SRA database, PRJNA928236). The number of genes differentially expressed respect to control cells were 207 in NOX2-silenced cells, 394 in NOX4-silenced cells, and 116 in the doubly NOX2/NOX4-silenced cells (Supplementary Fig. 5A). There were 30 genes in common between NOX2- and NOX4-silenced cells; and 60 and 34 genes in common between the doubly NOX2/NOX4-silenced cells with the single NOX2 and NOX4 silencing respectively (Supplementary Fig. 5A).

It is noteworthy that NOX4 silencing leads to the higher number of differentially expressed genes, suggesting the importance of this enzyme in the regulation of CML cells. On the other hand, it is also striking that the doubly NOX2/NOX4-silenced cells showed the shortest list of modified genes.

To delve into the meaning of these differences we looked for processes or pathways enrichment in the appropriate databases. In NOX2-silenced cells we found enrichment in several GO (Gene Ontology) terms related to metabolism (Fig. 9A and Supplementary Table IV), among the terms with the highest p-value stand out GO:0006090 (*pyruvate metabolic process*) or GO:0006096 (*glycolytic process*). Pathway analyses confirmed these results, where these pathways appeared among the most significantly altered (Supplementary Table V). This confirms the implication of NOX2 in the regulation of glucose energetic metabolism, in agreement with our experimental results, and suggest the implication of NOX2 in other metabolic processes such *lipid metabolism* or *glycosaminoglycan catabolism* (Fig. 9A).

In line with the reduced of NRF2 protein levels (Supplementary Fig. 5B), these transcriptomic analyses revealed the downregulation of *NRF2* mRNA and its signalling pathway in NOX2-silenced cells (Supplementary Fig. 5C).

Moreover, in agreement with the alteration of calcium homeostasis described above, we found several GO terms (GO:0006874_*cellular calcium ion homeostasis*, GO:0043647_*inositol phosphate metabolic process*, GO:0035584_*calcium-mediated signalling using intracellular calcium source*), and pathways (hsa04070, hsa04020, R-HSA-139853, R-HSA-1483249) altered in NOX2-silenced cells (Fig. 9A and Supplementary Table IV, V).

Regarding NOX4-silenced cells, as happened with NOX2-silenced cells, there were several GO terms (GO:0006094_*gluconeogenesis*,

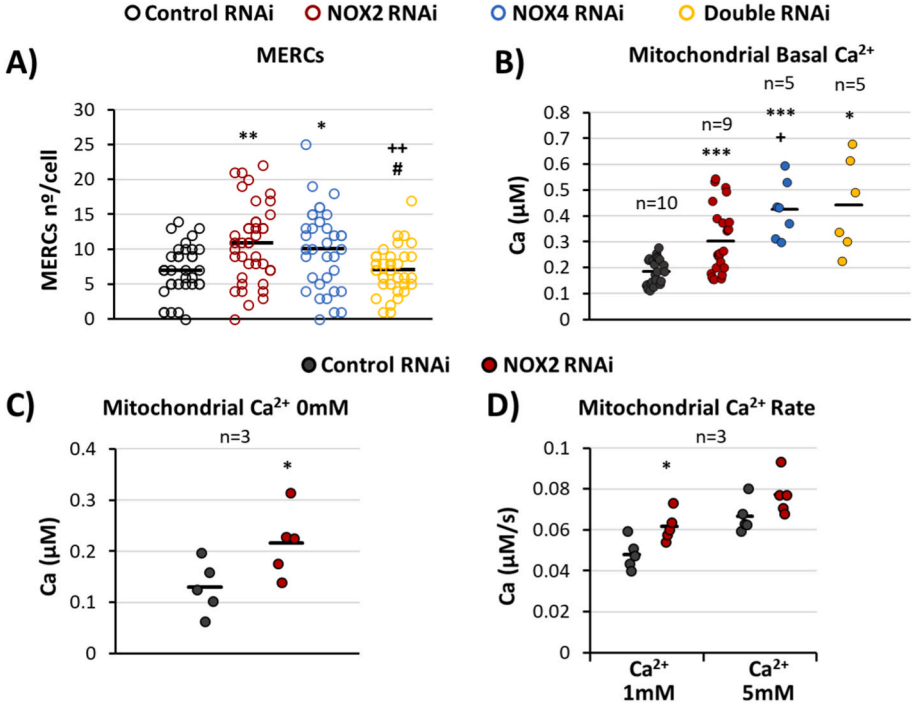

Fig. 8. Effect of NOX2 and NOX4 on MERCs and mitochondrial basal calcium. (A) The number of MERCs was monitored by TEM, as is described in the methods section, in control, NOX2-, NOX4-and NOX2/NOX4-doubly silenced K562 cells. The number of MERCs per cell is shown. **(B)** Basal $[Ca^{2+}]_M$ in external 1 mM Ca^{2+} medium of NOX2-, NOX4-, NOX2/NOX4-silenced and control cells. **(C)** Basal $[Ca^{2+}]_M$ in calcium-free medium of NOX2-silenced cells. **(D)** Mitochondrial calcium uptake rate upon SOCE stimulation in NOX2-silenced and control cells. The horizontal lines in graphs represent the mean of each parameter within each cell line. In B-D each point represents one independent experiment of n biological replicates. * Reflect significant differences versus control cells, + versus NOX2-silenced cells and # versus NOX4-silenced cells. For panel A–B two-way ANOVA test was used, for C-D two-way Student's T-Test was applied. Double RNAi, NOX2/NOX4-silenced cells; MERCs, mitochondrial-endoplasmic reticulum contacts; TEM, transmission electron microscopy; $[Ca^{2+}]_M$, mitochondrial calcium concentration; SOCE, store-operated calcium entry.

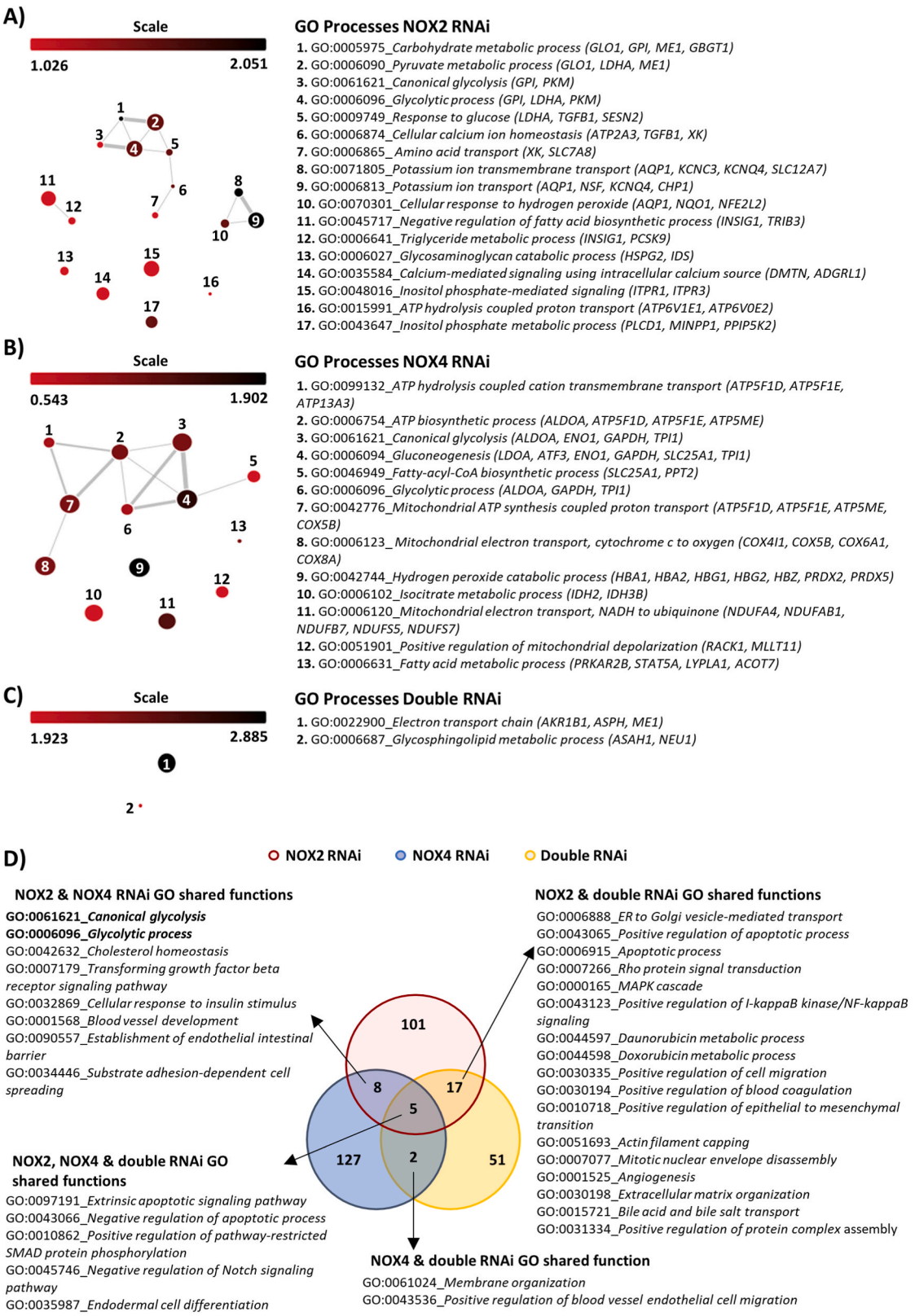

Fig. 9. GO metabolic processes altered in NOX2-, NOX4-and NOX2/NOX4-silenced cell lines. Network of GO processes significantly altered in NOX2-silenced **(A)**, NOX4-silenced **(B)** and NOX2/NOX4-silenced cells **(C)** related to metabolism and calcium signalling. Each node represents a functional category whose colour reflects the percentage of significantly altered genes in that category. The lines show related genes between functional categories, being their thickness proportional to the number of genes in common. The size of each circle is inversely proportional to its p-value. The numbers assigned to each circle refer to the GO processes listed to the right of each figure together with the genes altered. **(D)** Each circle includes the GO process significantly altered in each cell line and the common areas include the shared ones. GO common processes are cited and those related to metabolism are highlighted in bold. Control cells n = 3, NOX2-silenced cells n = 3, NOX4-silenced cells n = 2 and NOX2/NOX4-silenced cells n = 3 biological replicates. GO, Gene Ontology; Double RNAi, NOX2/NOX4-silenced cells. (For interpretation of the references to colour in this figure legend, the reader is referred to the Web version of this article.)

GO:0061621_*canonical glycolysis*, GO:0006096_*glycolytic process*), and pathways (M00003, R-HSA-70263, M00002, M00001, R-HSA-70171, R-HSA-70326, WP534) that relate NOX4 with glucose metabolism (Fig. 9B and Supplementary Table VI). Moreover, there were also several terms that relate NOX4 with the mitochondria and the metabolism of this organelle (Fig. 9B, Supplementary Table VI, VII), which agrees with our experimental results.

Finally, in the cells with the double NOX2/NOX4 silencing, in line with the shortest list of genes differentially expressed (Supplementary Fig. 5A), we found the lowest number of modified GO terms (Fig. 9C–D and Supplementary Table VIII) and pathways (Supplementary Table IX). Given that NOX2 silencing enhances NOX4 expression, the biological processes or pathways that depend on NOX4 expression, would not be altered in the doubly silenced cells, explaining the lower number of differentially expressed genes and pathways in the double silencing (Fig. 9D).

4. Discussion

During the last decade NADPH oxidases have emerged as key players in the regulation of cellular signalling. Their expression in all types of eukaryotic cells guarantees their relevance in the control of redox signalling. An interesting theme in the field is to dissect the particular functions of each NOX isoform, which would be highly dependent on the context.

Increased production of ROS and metabolic rewiring are two acknowledged hallmarks of cancer with important therapeutic implications [2,3]. NADPH oxidases can contribute to the excessive tumour cells ROS production, and recent evidence also relate these enzymes with the regulation of cancer metabolism [2].

Certain oncogenes, such *BCR-ABL*, simultaneously induce metabolic rewiring [3], and an increase of ROS [16] in tumour cells. This strongly suggests that both aspects are intimately related [2]. In addition, recent evidence support the relevance of NADPH oxidases, specially NOX2 and NOX4 in the regulation of cellular metabolism [2]. Moreover, NADPH oxidases driven ROS production is required to maintain BCR-ABL signalling [16,17]. Bearing all this in mind we thought worthwhile to analyse the role of NADPH oxidases in the regulation of CML cells metabolism. Here we have focused on NOX2, the main isoform in hematopoietic cells [43], and NOX4, an isoform which has been previously related with the control of mitochondrial metabolism [23]. By silencing the expression of NOX2, NOX4 and their common structurally required subunit $p22^{phox}$, we present evidence that support the relevance of both NADPH oxidases in the control of CML metabolism. Moreover, our data suggest the existence of a functional link between NOX2 and the mitochondria, that would be mediated through the regulation of NOX4 expression. As we have previously shown, NADPH oxidase driven ROS production is necessary to maintain BCR-ABL signalling [17]. Here we provide further evidence supporting a leading role of NOX2 in such signalling and at the same time, it suggests that the functional axis NOX2-NOX4-mitochondria may be under the control of BCR-ABL.

Here we show that NOX2 silencing increases glucose uptake and its flux through the glycolytic pathway, which is shunted to mitochondrial OXPHOS. To maintain a high rate of glycolysis, cells require NAD^+, that in the cytosol can be provided by lactic fermentation. However, although we detected an increase in LDH activity, there was not an increase of lactate, and on top of that, the proportion of ^{13}C-labelled lactate suggested that LDH might be rather oxidising lactate to pyruvate, and therefore reducing NAD^+/NADH ratio. In contrast we found that glycerol phosphate was virtually 100% ^{13}C-labelled, what strongly suggests that this metabolite comes from the reduction of the glycolytic intermediate glyceraldehyde 3-phosphate. This notion is also supported by the significant decrease of phosphoglycerate upon NOX2 silencing. This is consistent with the upregulation of the glycerol-phosphate shuttle, which would regenerate cytosolic NAD^+ necessary to support accelerated glycolysis, and transferring reductive power to the mitochondrial electron transport chain [3]. This is one factor explaining the higher mitochondrial metabolism displayed by NOX2-silenced cells. Besides pyruvate coming from glycolysis, our results suggest that NOX2-silenced cells also have a higher use of glutamine as a source of carbon for the TCA cycle.

Despite this apparent higher rate of metabolism, NOX2 silencing leads to a lower proliferation capacity. This could be related with a higher degree of mitochondrial stress, evidenced by the increase of mitochondrial ROS, the alteration of mtDNA CN, and $\Delta\Psi m$ decrease, which might make the cells more prone to apoptosis. Additionally, an unbalance between catabolism and anabolism could be also detrimental. Along this line, the increase of valine and the high labelling of glycerol phosphate upon NOX2 silencing would be consistent with an enhancement diversion of glucose to amino acid and lipid anabolism respectively. However, such increase in lipid anabolism is not supported by the inactivation of ACC, or the low flow of glucose through the PPP, suggesting an unbalanced metabolism upon NOX2 silencing.

Our results show a connection between NADPH oxidases and the mitochondria, the two main cellular sources of ROS, and support the importance of NOX2 to maintain mitochondrial homeostasis. NOX4 expression in the inner mitochondrial membrane has been previously described [23]. Our results are consistent with an increase of NOX4 expression in the mitochondria, what would facilitate the connection between NOX2 and the mitochondria. NOX2 silencing and imatinib treatment led to the upregulation of *NOX4* mRNA expression, suggesting that in CML cells *NOX4* transcription is under the control of BCR-ABL/NOX2 axis. An interesting issue would be to dissect which are the downstream signalling events doing the job. It has been previously described that AKT inhibition and the following GSK3β activation eventually lead to the enhancement of NOX4 expression [58]. The alterations of these pathways upon NOX2 silencing could explain the upregulation of NOX4.

Our results and those of others [45–48] show a cross-regulation between NOX2 and NOX4 in several different biological systems, suggesting that this might be a basic or general cellular phenomenon. If this was so, the axis NOX2/NOX4 might show particularities depending on the signalling context. In our case, we suggest that this regulation works under the umbrella of BCR-ABL signalling, and it would be then important for the onco-kinase to control leukemic cell metabolism and proliferation.

There exists the possibility of understanding the relation NOX2/NOX4 as a compensatory mechanism, the lack of a NOX isoform may be compensated by the upregulation of another isoform. However, there are certain particularities that make us stand against this notion. First, NOX2 and NOX4 show different subcellular locations [18], so it is hard to understand how the lack of one isoform would be compensated by the other. Second, while NOX4 is constitutively active [18], NOX2 must be activated, mainly by the phosphorylation of several cytoplasmic subunits [18]; therefore it seems unlikely that two isoforms with such a different mechanism of activation might substitute each other. And finally, even though its expression has not been described in the mitochondria, NOX2 silencing induces a dramatic alteration of the mitochondria, which could be mediated by NOX4, supporting the specificity of both NOXs.

NOX2 silencing induced an increase in OXPHOS activity, surprisingly accompanied by a decrease in mtDNA-encoded subunits of the respiratory chain. An interesting issue for future studies will be to investigate how NOX2 regulates this process, and whether NOX4 is involved. At this moment we can suggest that MFN2 downregulation upon NOX2 silencing might be part of the explanation, given that MFN2 downregulation suppresses the expression of several nuclear-encoded components of Complexes I, II, III and V, without affecting the mitochondrial content [59]. Moreover, MFN2 ablation results in depletion of mtDNA CN, an event we have observed in NOX2-silenced cells. On the other hand, the effects of MFN2 on mitochondrial metabolism seem to depend on the context, with reports showing that MFN2 depletion could

induce either a decrease [59], or an increase [60] in mitochondrial respiration. Whether MFN2 is involved in the upregulation of OXPHOS in our system is a possibility worthwhile to analyse in the future.

Ca^{2+} transfer from the ER to the mitochondria is required to control metabolism through the activation of several TCA cycle enzymes, the ATPase and aspartate and glutamate transporters [61]. However, an overload of Ca^{2+} can be detrimental to OXPHOS, increasing the risk of mitochondrial permeability transition pore formation and apoptosis [62]. The higher $[Ca^{2+}]_M$ detected in NOX2-and NOX4-silenced cells in comparison to control cells could be related with the increased number of MERCs. However, we cannot say the same for the double NOX2/NOX4-silenced cells. An alternative explanation for the case of the doubly silenced would be the downregulation of MFN2, which has previously been described to enhance Ca^{2+} transfer from the ER to the mitochondria by inducing the elongation of MERCs without affecting their number [63].

It is tempting to suggest that an increase of $mtCa^{2+}$ in NOX2-silenced cells might contribute significantly to the OXPHOS activation, while a $mtCa^{2+}$ overload displayed by NOX4- and the doubly NOX2/NOX4-silenced might be detrimental to OXPHOS metabolism.

BCR-ABL inhibition induces a shift from glycolytic to OXPHOS metabolism, and the downregulation of PPP [11]. Such changes recall the alterations here described for NOX2-silenced cells. In addition, and in agreement with our previous results [17], we show the implication of NOX2 in the maintenance of BCR-ABL signalling. All in all, our results are consistence with the relevance of NOX2 in the regulation of metabolism by BCR-ABL.

Moreover, we present evidence supporting a functional connection between the two main cellular sources of ROS, the NADPH oxidases and the mitochondria. NOX2, by regulating NOX4 expression, modulates mitochondrial function, structure and bioenergetics capacity. Such functional axis might not be exclusive of CML cells, as suggested by the regulation of NOX4 expression by NOX2 in other biological systems [45, 46], and it might reflect a general biological phenomenon. To fully understand the molecular mechanisms sustaining the axis NOX2-NOX4-mitochondria is an interesting challenge for the future, that in the CML field will pave the way to the development of novel therapeutic strategies.

5. Conclusions

Our results support the existence of a NOX2-NOX4-mitochondria functional axis involved in the regulation of CML bioenergetics. Silencing of NOX2 enhances glycolytic and OXPHOS rates in CML cells, but simultaneously induces mitochondrial stress. Upregulation of NOX4 upon NOX2 silencing seems a key even to functionally connect NOX2 and mitochondria. NOX2 silencing alters metabolism-related signalling pathways downstream of BCR-ABL. Our results suggest the existence of a functional axis NOX2-NOX4-mitochondria in the CML context, and sustain the importance of these NADPH oxidases in the regulation of metabolism mediated by the oncogene *BCR-ABL*.

Funding sources

Marta Romo-González and Carla Ijurko were recipient of predoctoral fellowships from the Regional Government of Castile and Leon, Spain and ERDF funds. Funding sources were as follows: Angel Hernández-Hernández lab: Spanish Government (PID2020-117692RB-I00), Regional Government of Castile & Leon (SA077P20) and Ramón Areces Foundation (CIV17A2822). Ana Ramirez de Molina lab: Spanish Government (PID2019-110183RB-C21), Regional Government of Community of Madrid (P2018/BAA-4343-ALIBIRD2020-CM), Synergistic Projects Community of Madrid NUTRISION-CM/Y2020/BIO-6350. Maria Teresa Alonso lab: Spanish Government (PID2020-116086RB-I00).

Authors contributions

MRG performed experiments, analysed data, assemble figures and wrote the manuscript. CI analysed data and revised the manuscript. MTA designed Ca^{2+} analyses experiments. MGC performed experiments and revised the manuscript. ARM revised the manuscript. MES designed mitochondrial structure and function experiments. AHH conceived and designed experiments, analysed data and wrote the manuscript.

Disclosure of conflicts of interest

The authors declare no conflict of interest.

Acknowledgements

We thank the Mass Spectrometry Facility of the University of Salamanca and the Microscopy Facility of the University of Padua for their technical support. We would like to thank Dr. Ulla Knaus (University College Dublin), who kindly provided NOX4 antibody.

Appendix A. Supplementary data

Supplementary data to this article can be found online at https://doi.org/10.1016/j.freeradbiomed.2023.02.005.

References

[1] O. Warburg, On the origin of cancer cells, Science 80 (123) (1956) 309–314, https://doi.org/10.1126/science.123.3191.309.
[2] M. Romo-González, C. Ijurko, Á. Hernández-Hernández, Reactive oxygen species and metabolism in leukemia: a dangerous liaison, Front. Immunol. 13 (2022), https://doi.org/10.3389/FIMMU.2022.889875.
[3] R. Prieto-Bermejo, M. Romo-González, A. Pérez-Fernández, C. Ijurko, Á. Hernández-Hernández, Reactive oxygen species in haematopoiesis: leukaemic cells take a walk on the wild side, J. Exp. Clin. Cancer Res. 37 (2018) 1–18, https://doi.org/10.1186/s13046-018-0797-0.
[4] M. Koptyra, R. Falinski, M.O. Nowicki, T. Stoklosa, I. Majsterek, M. Nieborowska-Skorska, J. Blasiak, T. Skorski, BCR/ABL kinase induces self-mutagenesis via reactive oxygen species to encode imatinib resistance, Blood 108 (2006) 319–327, https://doi.org/10.1182/blood-2005-07-2815.
[5] K. Irani, Y. Xia, J.L. Zweier, S.J. Sollott, C.J. Der, E.R. Fearon, M. Sundaresan, T. Finkel, P.J. Goldschmidt-Clermont, Mitogenic signaling mediated by oxidants in Ras-transformed fibroblasts, Science 275 (1997) 1649–1652, https://doi.org/10.1126/science.275.5306.1649.
[6] A. Nakanishi, Y. Wada, Y. Kitagishi, S. Matsuda, Link between PI3K/AKT/PTEN pathway and NOX protein in diseases, Aging Dis 5 (2014) 203–211, https://doi.org/10.14336/AD.2014.0500203.
[7] S. Trombetti, E. Cesaro, R. Catapano, R. Sessa, A. Lo Bianco, P. Izzo, M. Grosso, Oxidative stress and ROS-mediated signaling in leukemia: novel promising perspectives to eradicate chemoresistant cells in myeloid leukemia, Int. J. Mol. Sci. 22 (2021) 1–19, https://doi.org/10.3390/IJMS22052470.
[8] L. de Beauchamp, E. Himonas, G.V. Helgason, Mitochondrial metabolism as a potential therapeutic target in myeloid leukaemia, Leukemia 36 (2022), https://doi.org/10.1038/S41375-021-01416-W.
[9] J.R. Sillar, Z.P. Germon, G.N. De Iuliis, M.D. Dun, The role of reactive oxygen species in acute myeloid leukaemia, Int. J. Mol. Sci. 20 (2019) 1–20, https://doi.org/10.3390/ijms20236003.
[10] B. Chereda, J.V. Melo, Natural course and biology of CML, Ann. Hematol. 94 (2015) 107–121, https://doi.org/10.1007/s00277-015-2325-z.
[11] V. De Rosa, M. Monti, C. Terlizzi, R. Fonti, S. Del Vecchio, F. Iommelli, Coordinate modulation of glycolytic enzymes and OXPHOS by imatinib in BCR-ABL driven chronic myelogenous leukemia cells, Int. J. Mol. Sci. 20 (2019), https://doi.org/10.3390/IJMS20133134.
[12] S. Zhou, X. Zhu, W. Liu, F. Cheng, P. Zou, Y. You, Y. Xiao, A. Guo, X. Zhu, Comparison of chronic myeloid leukemia stem cells and hematopoietic stem cells by global proteomic analysis, Biochem. Biophys. Res. Commun. 522 (2020) 362–367, https://doi.org/10.1016/J.BBRC.2019.11.092.
[13] J.H. Kim, S.C. Chu, J.L. Gramlich, Y.B. Pride, E. Babendreier, D. Chauhan, R. Salgia, K. Podar, J.D. Griffin, M. Sattler, Activation of the PI3K/mTOR pathway by BCR-ABL contributes to increased production of reactive oxygen species, Blood 105 (2005) 1717–1723, https://doi.org/10.1182/blood-2004-03-0849.
[14] M. Sattler, S. Verma, G. Shrikhande, C.H. Byrne, Y.B. Pride, T. Winkler, E. A. Greenfield, R. Salgia, J.D. Griffin, The BCR/ABL tyrosine kinase induces production of reactive oxygen species in hematopoietic cells, J. Biol. Chem. 275 (2000) 24273–24278, https://doi.org/10.1074/jbc.M002094200.
[15] M. Romo-González, S. Moreno-Paz, V. García-Hernández, F. Sánchez-Guijo, Á. Hernández-Hernández, Inhibition of xanthine oxidoreductase enhances the

potential of tyrosine kinase inhibitors against chronic myeloid leukemia, Antioxidants 9 (2020), https://doi.org/10.3390/antiox9010074.
[16] R. Naughton, C. Quiney, S.D. Turner, T.G. Cotter, Bcr-Abl-mediated redox regulation of the PI3K/AKT pathway, Leukemia 23 (2009) 1432–1440, https://doi.org/10.1038/leu.2009.49.
[17] B. Sánchez-Sánchez, S. Gutiérrez-Herrero, G. López-Ruano, R. Prieto-Bermejo, M. Romo-González, M. Llanillo, A. Pandiella, C. Guerrero, J.F. San Miguel, F. Sánchez-Guijo, C. Del Cañizo, A. Hernández-Hernández, NADPH oxidases as therapeutic targets in chronic myelogenous leukemia, Clin. Cancer Res. 20 (2014) 4014–4025, https://doi.org/10.1158/1078-0432.CCR-13-3044.
[18] H. Buvelot, V. Jaquet, K.H. Krause, Mammalian NADPH oxidases, Methods Mol. Biol. 1982 (2019) 17–36, https://doi.org/10.1007/978-1-4939-9424-3_2.
[19] C. Prata, T. Maraldi, D. Fiorentini, L. Zambonin, G. Hakim, L. Landi, Nox-generated ROS modulate glucose uptake in a leukaemic cell line, Free Radic. Res. 42 (2008) 405–414, https://doi.org/10.1080/10715760802047344.
[20] W. Lu, Y. Hu, G. Chen, Z. Chen, H. Zhang, F. Wang, L. Feng, H. Pelicano, H. Wang, M.J. Keating, J. Liu, W. McKeehan, H. Wang, Y. Luo, P. Huang, Novel role of NOX in supporting aerobic glycolysis in cancer cells with mitochondrial dysfunction and as a potential target for cancer therapy, PLoS Biol. 10 (2012), e1001326, https://doi.org/10.1371/journal.pbio.1001326.
[21] A. Baillet, M.A. Hograindleur, J. El Benna, A. Grichine, S. Berthier, F. Morel, M. H. Paclet, Unexpected function of the phagocyte NADPH oxidase in supporting hyperglycolysis in stimulated neutrophils: key role of 6-phosphofructo-2-kinase, Faseb. J. 31 (2017) 663–673, https://doi.org/10.1096/fj.201600720R.
[22] A.J. Robinson, G.L. Hopkins, N. Rastogi, M. Hodges, M. Doyle, S. Davies, P.S. Hole, N. Omidvar, R.L. Darley, A. Tonks, Reactive oxygen species drive proliferation in acute myeloid leukemia via the glycolytic regulator PFKFB3, Cancer Res. 80 (2020) 937–949, https://doi.org/10.1158/0008-5472.CAN-19-1920.
[23] K. Shanmugasundaram, B.K. Nayak, W.E. Friedrichs, D. Kaushik, R. Rodriguez, K. Block, NOX4 functions as a mitochondrial energetic sensor coupling cancer metabolic reprogramming to drug resistance, Nat. Commun. 8 (2017) 1–15, https://doi.org/10.1038/s41467-017-01106-1.
[24] K. Bernard, N.J. Logsdon, V. Miguel, G.A. Benavides, J. Zhang, A.B. Carter, V. M. Darley-Usmar, V.J. Thannickal, NADPH Oxidase 4 (Nox4) suppresses mitochondrial biogenesis and bioenergetics in lung fibroblasts via a nuclear factor erythroid-derived 2-like 2 (Nrf2)-dependent pathway, J. Biol. Chem. 292 (2017) 3029–3038, https://doi.org/10.1074/jbc.M116.752261.
[25] J.L. Sardina, G. López-Ruano, R. Prieto-Bermejo, B. Sánchez-Sánchez, A. Pérez-Fernández, L.I. Sánchez-Abarca, J.A. Pérez-Simón, L. Quintales, J. Sánchez-Yagüe, M. Llanillo, F. Antequera, A. Hernández-Hernández, PTPN13 regulates cellular signalling and β-catenin function during megakaryocytic differentiation, Biochim. Biophys. Acta 1843 (2014) 2886–2899, https://doi.org/10.1016/J.BBAMCR.2014.08.014.
[26] G. López-Ruano, R. Prieto-Bermejo, T.L. Ramos, L. San-Segundo, L.I. Sánchez-Abarca, F. Sánchez-Guijo, J.A. Pérez-Simón, J. Sánchez-Yagüe, M. Llanillo, Á. Hernández-Hernández, PTPN13 and β-catenin regulate the quiescence of hematopoietic stem cells and their interaction with the bone marrow niche, Stem Cell Rep. 5 (2015) 516–531, https://doi.org/10.1016/J.STEMCR.2015.08.003.
[27] N.R. Phillips, M.L. Sprouse, R.K. Roby, Simultaneous quantification of mitochondrial DNA copy number and deletion ratio: a multiplex real-time PCR assay, Sci. Rep. 4 (2014), https://doi.org/10.1038/SREP03887.
[28] C. Frezza, S. Cipolat, L. Scorrano, Organelle isolation: functional mitochondria from mouse liver, muscle and cultured fibroblasts, Nat. Protoc. 2 (2007) 287–295, https://doi.org/10.1038/NPROT.2006.478.
[29] S. O'Neill, M. Mathis, L. Kovačič, S. Zhang, J. Reinhardt, D. Scholz, U. Schopfer, R. Bouhelal, U.G. Knaus, Quantitative interaction analysis permits molecular insights into functional NOX4 NADPH oxidase heterodimer assembly, J. Biol. Chem. 293 (2018) 8750–8760, https://doi.org/10.1074/JBC.RA117.001045.
[30] C.A. Sellick, R. Hansen, G.M. Stephens, R. Goodacre, A.J. Dickson, Metabolite extraction from suspension-cultured mammalian cells for global metabolite profiling, Nat. Protoc. 6 (2011) 1241–1249, https://doi.org/10.1038/nprot.2011.366.
[31] C. Glytsou, E. Calvo, S. Cogliati, A. Mehrotra, I. Anastasia, G. Rigoni, A. Raimondi, N. Shintani, M. Loureiro, J. Vazquez, L. Pellegrini, J.A. Enriquez, L. Scorrano, M. E. Soriano, Optic atrophy 1 is epistatic to the core MICOS component MIC60 in mitochondrial cristae shape control, Cell Rep. 17 (2016) 3024–3034, https://doi.org/10.1016/j.celrep.2016.11.049.
[32] R. Prieto-Bermejo, M. Romo-González, A. Pérez-Fernández, I. García-Tuñón, M. Sánchez-Martín, Á. Hernández-Hernández, Cyba-deficient mice display an increase in hematopoietic stem cells and an overproduction of immunoglobulins, Haematologica 106 (2021) 142–153, https://doi.org/10.3324/haematol.2019.233064.
[33] M.T. Alonso, M. Rodríguez-Prados, P. Navas-Navarro, J. Rojo-Ruiz, J. García-Sancho, Using aequorin probes to measure Ca2+ in intracellular organelles, Cell Calcium 64 (2017) 3–11, https://doi.org/10.1016/J.CECA.2017.01.006.
[34] M.M. Reddy, M.S. Fernandes, R. Salgia, R.L. Levine, J.D. Griffin, M. Sattler, NADPH oxidases regulate cell growth and migration in myeloid cells transformed by oncogenic tyrosine kinases, Leukemia 25 (2011) 281–289, https://doi.org/10.1038/leu.2010.263.
[35] C.A. Castellani, R.J. Longchamps, J. Sun, E. Guallar, D.E. Arking, Thinking outside the nucleus: mitochondrial DNA copy number in health and disease, Mitochondrion 53 (2020) 214–223, https://doi.org/10.1016/J.MITO.2020.06.004.
[36] G. Cecchini, Function and structure of complex II of the respiratory chain, Annu. Rev. Biochem. 72 (2003) 77–109, https://doi.org/10.1146/ANNUREV.BIOCHEM.72.121801.161700.
[37] B.A. Hemmings, D.F. Restuccia, PI3K-PKB/Akt pathway, Cold Spring Harbor Perspect. Biol. 4 (2012), https://doi.org/10.1101/CSHPERSPECT.A011189.
[38] B. Markova, C. Albers, F. Breitenbuecher, J.V. Melo, T.H. Brümmendorf, F. Heidel, D. Lipka, J. Duyster, C. Huber, T. Fischer, Novel pathway in Bcr-Abl signal transduction involves Akt-independent, PLC-gamma1-driven activation of mTOR/p70S6-kinase pathway, Oncogene 29 (2010) 739–751, https://doi.org/10.1038/ONC.2009.374.
[39] S.J. Forrester, D.S. Kikuchi, M.S. Hernandes, Q. Xu, K.K. Griendling, Reactive oxygen species in metabolic and inflammatory signaling, Circ. Res. 122 (2018) 877–902, https://doi.org/10.1161/CIRCRESAHA.117.311401.
[40] K.G. de la Cruz López, M.E. Toledo Guzmán, E.O. Sánchez, A. García Carrancá, mTORC1 as a regulator of mitochondrial functions and a therapeutic target in cancer, Front. Oncol. 9 (2019), https://doi.org/10.3389/FONC.2019.01373.
[41] F. Chiara, A. Rasola, GSK-3 and mitochondria in cancer cells, Front. Oncol. 3 (2013), https://doi.org/10.3389/FONC.2013.00016.
[42] S.K. Niture, R. Khatri, A.K. Jaiswal, Regulation of nrf2-an update, Free Radic. Biol. Med. 66 (2014) 36–44, https://doi.org/10.1016/J.FREERADBIOMED.2013.02.008.
[43] H. Dakik, M. El Dor, J. Leclerc, F. Kouzi, A. Nehme, M. Deynoux, C. Debeissat, G. Khamis, E. Ducrocq, A. Ibrik, M.J. Stasia, H. Raad, H.R. Rezvani, F. Gouilleux, K. Zibara, O. Herault, F. Mazurier, Characterization of NADPH oxidase expression and activity in acute myeloid leukemia cell lines: a correlation with the differentiation status, Antioxidants 10 (2021) 498, https://doi.org/10.3390/antiox10030498.
[44] K.A. Graham, M. Kulawiec, K.M. Owens, X. Li, M.M. Desouki, D. Chandra, K. K. Singh, NADPH oxidase 4 is an oncoprotein localized to mitochondria, Cancer Biol. Ther. 10 (2010) 223–231, https://doi.org/10.4161/cbt.10.3.12207.
[45] T.R. Cully, G.G. Rodney, Nox4 – RyR1 – Nox2: regulators of micro-domain signaling in skeletal muscle, Redox Biol. 36 (2020), 101557, https://doi.org/10.1016/J.REDOX.2020.101557.
[46] V. Helfinger, K. Palfi, A. Weigert, K. Schröder, The NADPH oxidase Nox4 controls macrophage polarization in an NFκB-dependent manner, Oxid. Med. Cell. Longev. 2019 (2019), https://doi.org/10.1155/2019/3264858.
[47] S. Pendyala, I.A. Gorshkova, P.V. Usatyuk, D. He, A. Pennathur, J.D. Lambeth, V. J. Thannickal, V. Natarajan, Role of Nox4 and Nox2 in hyperoxia-induced reactive oxygen species generation and migration of human lung endothelial cells, Antioxid, Redox Signal 11 (2009) 747–764, https://doi.org/10.1089/ARS.2008.2203.
[48] S.P. Gray, E. Di Marco, K. Kennedy, P. Chew, J. Okabe, A. El-Osta, A.C. Calkin, E.A. L. Biessen, R.M. Touyz, M.E. Cooper, H.H.H.W. Schmidt, K.A.M. Jandeleit-Dahm, Reactive oxygen species can provide atheroprotection via NOX4-dependent inhibition of inflammation and vascular remodeling, Arterioscler. Thromb. Vasc. Biol. 36 (2016) 295–307, https://doi.org/10.1161/ATVBAHA.115.307012.
[49] I. Peñuelas-Haro, R. Espinosa-Sotelo, E. Crosas-Molist, M. Herranz-Itúrbide, D. Caballero-Díaz, A. Alay, X. Solé, E. Ramos, T. Serrano, M.L. Martínez-Chantar, U.G. Knaus, J.M. Cuezva, A. Zorzano, E. Bertran, I. Fabregat, The NADPH oxidase NOX4 regulates redox and metabolic homeostasis preventing HCC progression, Hepatology (2022), https://doi.org/10.1002/HEP.32702.
[50] I. Diebold, A. Petry, J. Hess, A. Gorlach, The NADPH oxidase subunit NOX4 is a new target gene of the hypoxia-inducible factor-1, Mol. Biol. Cell 21 (2010) 2087–2096.
[51] G. Bai, T.D. Hock, N. Logsdon, Y. Zhou, V.J. Thannickal, A far-upstream AP-1/Smad binding box regulates human NOX4 promoter activation by transforming growth factor-β, Gene 540 (2014) 62–67, https://doi.org/10.1016/J.GENE.2014.02.026.
[52] M. Katsuyama, H. Hirai, K. Iwata, M. Ibi, K. Matsuno, M. Matsumoto, C. Yabe-Nishimura, Sp3 transcription factor is crucial for transcriptional activation of the human NOX4 gene, FEBS J. 278 (2011) 964–972, https://doi.org/10.1111/J.1742-4658.2011.08018.X.
[53] C. Hirschhäuser, J. Bornbaum, A. Reis, S. Böhme, N. Kaludercic, R. Menabò, F. Di Lisa, K. Boengler, A.M. Shah, R. Schulz, H.H.H.W. Schmidt, NOX4 in mitochondria: yeast two-hybrid-based interaction with complex I without relevance for basal reactive oxygen species? Antioxidants Redox Signal. 23 (2015) 1106–1112, https://doi.org/10.1089/ars.2014.6238.
[54] S. Cogliati, C. Frezza, M.E. Soriano, T. Varanita, R. Quintana-Cabrera, M. Corrado, S. Cipolat, V. Costa, A. Casarin, L.C. Gomes, E. Perales-Clemente, L. Salviati, P. Fernandez-Silva, J.A. Enriquez, L. Scorrano, Mitochondrial cristae shape determines respiratory chain supercomplexes assembly and respiratory efficiency, Cell 155 (2013) 160–171, https://doi.org/10.1016/j.cell.2013.08.032.
[55] D.W. Hailey, A.S. Rambold, P. Satpute-Krishnan, K. Mitra, R. Sougrat, P.K. Kim, J. Lippincott-Schwartz, Mitochondria supply membranes for autophagosome biogenesis during starvation, Cell 141 (2010) 656–667, https://doi.org/10.1016/J.CELL.2010.04.009.
[56] J. Kadkhoda, A. Tarighatnia, N.D. Nader, A. Aghanejad, Targeting mitochondria in cancer therapy: insight into photodynamic and photothermal therapies, Life Sci. 307 (2022), https://doi.org/10.1016/J.LFS.2022.120898.
[57] M. Giacomello, L. Pellegrini, The coming of age of the mitochondria-ER contact: a matter of thickness, Cell Death Differ. 23 (2016) 1417–1427, https://doi.org/10.1038/CDD.2016.52.
[58] Q. Yang, L. Wen, Z. Meng, Y. Chen, Blockage of endoplasmic reticulum stress attenuates nilotinib-induced cardiotoxicity by inhibition of the Akt-GSK3β-Nox4 signaling, Eur. J. Pharmacol. 822 (2018) 85–94, https://doi.org/10.1016/J.EJPHAR.2018.01.011.
[59] S. Pich, D. Bach, P. Briones, M. Liesa, M. Camps, X. Testar, M. Palacín, A. Zorzano, The Charcot-Marie-Tooth type 2A gene product, Mfn2, up-regulates fuel oxidation

through expression of OXPHOS system, Hum. Mol. Genet. 14 (2005) 1405–1415, https://doi.org/10.1093/HMG/DDI149.
[60] M. Kawalec, A. Boratyńska-Jasińska, M. Beresewicz, D. Dymkowska, K. Zabłocki, B. Zabłocka, Mitofusin 2 deficiency affects energy metabolism and mitochondrial biogenesis in MEF cells, PLoS One 10 (2015), https://doi.org/10.1371/journal.pone.0134162.
[61] C. Fernandez-Sanz, S. De la Fuente, S.S. Sheu, Mitochondrial Ca2+ concentrations in live cells: quantification methods and discrepancies, FEBS Lett. 593 (2019) 1528–1541, https://doi.org/10.1002/1873-3468.13427.
[62] J.O. Strubbe-Rivera, J. Chen, B.A. West, K.N. Parent, G.-W. Wei, J.N. Bazil, Modeling the effects of calcium overload on mitochondrial ultrastructural remodeling, Appl. Sci. 11 (2021) 2071, https://doi.org/10.3390/APP11052071.
[63] N.S. Leal, B. Schreiner, C.M. Pinho, R. Filadi, B. Wiehager, H. Karlström, P. Pizzo, M. Ankarcrona, Mitofusin-2 knockdown increases ER–mitochondria contact and decreases amyloid β-peptide production, J. Cell Mol. Med. 20 (2016) 1686–1695, https://doi.org/10.1111/jcmm.12863.